Global Biogeochemical Cycles

RESEARCH ARTICLE
10.1029/2021GB007196

Key Points:

- The western margin and southern limit of the South Atlantic Ocean are more impacted by anthropogenic carbon (C_{ant}) uptake
- A C_{ant} column inventory change of 0.94 ± 0.39 mol C m^{-2} yr^{-1} was found in the region, higher than the global mean storage rate
- Aragonite unsaturation is expected in the next two decades along the eastern margin if the anthropogenic changes maintain the present trend

Supporting Information:

Supporting Information may be found in the online version of this article.

Correspondence to:

A. Piñango and R. Kerr,
andreseloy@furg.br;
rodrigokerr@furg.br

Citation:

Piñango, A., Kerr, R., Orselli, I. B. M., Carvalho, A. C. O., Azar, E., Karstensen, J., & Garcia, C. A. E. (2022). Ocean acidification and long-term changes in the carbonate system properties of the South Atlantic Ocean. *Global Biogeochemical Cycles*, *36*, e2021GB007196. https://doi.org/10.1029/2021GB007196

Received 18 SEP 2021
Accepted 25 AUG 2022

Author Contributions:

Conceptualization: Andrés Piñango, Rodrigo Kerr, Iole Beatriz Marques Orselli, Andréa da Consolação Oliveira Carvalho, Elias Azar
Data curation: Andrés Piñango
Formal analysis: Andrés Piñango
Funding acquisition: Rodrigo Kerr, Carlos Alberto Eiras Garcia
Investigation: Andrés Piñango
Methodology: Andrés Piñango, Rodrigo Kerr, Iole Beatriz Marques Orselli, Elias Azar

Ocean Acidification and Long-Term Changes in the Carbonate System Properties of the South Atlantic Ocean

Andrés Piñango[1,2,3], Rodrigo Kerr[1,2,3], Iole Beatriz Marques Orselli[1,2,3], Andréa da Consolação Oliveira Carvalho[1,2,3], Elias Azar[3], Johannes Karstensen[4], and Carlos Alberto Eiras Garcia[1,3]

[1]Laboratório de Estudos dos Oceanos e Clima—LEOC, Instituto de Oceanografia, Universidade Federal do Rio Grande—FURG, Rio Grande, Brazil, [2]Brazilian Ocean Acidification Network—BrOA, Rio Grande, Brazil, [3]Programa de Pós-Graduação em Oceanologia—PPGO, Instituto de Oceanografia, Universidade Federal do Rio Grande—FURG, Campus Carreiros, Rio Grande, Brazil, [4]GEOMAR Helmholtz Centre for Ocean Research Kiel, Kiel, Germany

Abstract The wind-driven part of the South Atlantic Ocean is primarily ventilated through central and intermediate water formation. Through the water mass formation processes, anthropogenic carbon (C_{ant}) is introduced into the ocean's interior which in turn makes the South Atlantic region vulnerable to ocean acidification. C_{ant} and the accompanying acidification effects have been estimated for individual sections in the region since the 1980s but a comprehensive synthesis for the entire basin is still lacking. Here, we quantified the C_{ant} accumulation rates and examined the changes in the carbonate system properties for the South Atlantic using a modified extended multiple linear regression method applied to five hydrographic sections and data from the GLODAPv2.2021 product. From 1989 to 2019, a mean C_{ant} column inventory change of 0.94 ± 0.39 mol C m^{-2} yr^{-1} was found. C_{ant} accumulation rates of 0.89 ± 0.33 μmol kg^{-1} yr^{-1} and 0.30 ± 0.29 μmol kg^{-1} yr^{-1} were observed in central and intermediate waters, accompanied by acidification rates of -0.0020 ± 0.0007 pH units yr^{-1} and -0.0009 ± 0.0009 pH units yr^{-1}, respectively. Furthermore, increased remineralization was observed in intermediate waters, amplifying the acidification of this water mass, especially at the African coast along 25°S. This increase in remineralization is likely related to circulation changes and increased biological activity nearshore. Assuming no changes in the observed trends, South Atlantic intermediate waters will become unsaturated with respect to aragonite in ~30 years, while the central water of the eastern margins will become unsaturated in ~10 years.

1. Introduction

Multiple human activities, such as the burning of fossil fuels and changes in the use of soils (e.g., deforestation), were responsible for the release of 700 ± 75 Pg C to the atmosphere from the Industrial Era (~1750) until the year 2019 (Friedlingstein et al., 2020). Approximately 41% of this anthropogenic carbon (C_{ant}) has remained in the atmosphere, increasing the concentration of carbon dioxide (CO_2) from 277 parts per million (ppm) in 1750 to 414.73 ± 0.10 ppm in 2021 (Dlugokencky & Tans, 2022). This excess of CO_2 has been causing changes in the radiative balance of the Earth and consequently in the climate system (Cubasch et al., 2013). The remaining C_{ant} (57%) has been captured by the terrestrial biosphere and the oceans (Friedlingstein et al., 2020), mitigating part of the changes in the Earth's climate.

In the ocean, the uptake of C_{ant} occurs at the surface by air-sea gas exchange, primarily driven by the solubility pump (Broecker, 1991; Sarmiento & Gruber, 2006). Thus, the C_{ant} uptake and storage are closely related to water mass formation. Indeed, a clear linkage has been identified between central, intermediate, and deep water masses transport and the storage of C_{ant} in the ocean interior (Gruber, Clement, et al., 2019; Sabine et al., 2004). The uptake, export, and storage of C_{ant} depend on ocean ventilation, ocean circulation, water mass properties, ocean-atmosphere interactions, mesoscale dynamics, and biogeochemical processes, resulting in a non-uniform C_{ant} distribution throughout the ocean basins (Gruber, Clement, et al., 2019; Lee et al., 2003; Sabine et al., 2004).

The South Atlantic Ocean is characterized by the intense formation of mode and intermediate waters (the former embedded in the central waters). These water masses are advected northward with the wind-driven subtropical gyre in what is termed the central and intermediate layers of the South Atlantic Ocean, and they provide the main pathway between the ocean surface and interior (Azar et al., 2021; de Souza et al., 2018; Stramma & England, 1999; Tanhua et al., 2017). In this region, recent estimates have found an increase in the C_{ant} inventory

Project Administration: Rodrigo Kerr
Resources: Rodrigo Kerr, Johannes Karstensen, Carlos Alberto Eiras Garcia
Software: Andrés Piñango
Supervision: Rodrigo Kerr, Iole Beatriz Marques Orselli
Validation: Andrés Piñango
Visualization: Andrés Piñango, Elias Azar
Writing – original draft: Andrés Piñango, Rodrigo Kerr, Elias Azar
Writing – review & editing: Andrés Piñango, Rodrigo Kerr, Iole Beatriz Marques Orselli, Andréa da Consolação Oliveira Carvalho, Johannes Karstensen, Carlos Alberto Eiras Garcia

of 5.3 ± 1.2 Pg C up to 3000 m between 1994 and 2007 (Gruber, Clement, et al., 2019) and a less variable C_{ant} decadal increase has been observed in comparison with the North Atlantic Ocean (Wanninkhof et al., 2010; Woosley et al., 2016).

The uptake of C_{ant} alters the equilibrium of the ocean's carbonate system, reducing the carbonate concentration (and the OH^-) and increasing the concentration of H^+ ions, which in the long-term results in a process known as ocean acidification (Doney, Balch, et al., 2009). Ocean acidification, known as "the other CO2 problem" (Doney, Fabry, et al., 2009), is a process observed on a global scale in multiple measurements (e.g., Feely et al., 2009; Lauvset et al., 2020; Orr et al., 2005; Takahashi et al., 2014). The alterations in the marine carbonate chemistry have the potential to disrupt entire ecosystems and calcifying organisms, such as pteropods, coccolithophorids, and coral reefs are especially susceptible to decreased calcite and aragonite saturation states (Ω_{Ca} and Ω_{Ar}, respectively) (Doney et al., 2020; Feely et al., 2009; Millero, 2007; Orr et al., 2005). Evidence from the geological record shows that multiple ocean acidification events have occurred in the past 300 million years, associated with significant losses of biodiversity and mass extinctions (Honisch et al., 2012).

Estimates of the C_{ant} content in the South Atlantic Ocean dates back to the 1980s (e.g., Chen, 1982). Based on repeat section analysis, open ocean acidification rates in central (-0.0020 pH units yr^{-1}) and intermediate (-0.0010 pH units yr^{-1}) water masses have been reported (e.g., Carvalho-Borges et al., 2018; Kitidis et al., 2017; Orselli et al., 2018; Ríos et al., 2015; Salt et al., 2015; Woosley et al., 2016). However, most of these studies have focused on specific sub-basins, as the distribution of oceanographic data for the entire region is uneven, especially over time. For example, Fontela et al. (2021) provided a detailed evaluation of the carbonate system variability in the Argentine Basin (western South Atlantic Ocean) over the last five decades, finding a decreasing carbonate concentration as consequence of C_{ant} uptake enhanced by the remineralization of organic matter in the intermediate layer. However, no such study exists for the eastern South Atlantic margin. With the completion of new hydrographic surveys in recent years (e.g., A9.5 at 24°S) and considering also repeat sections in the framework of the Global Ocean Ship-based Hydrographic Investigations Program (GO-SHIP), it is now possible to assess changes in the carbonate system properties for the entire basin.

Here, we evaluated the changes in the C_{ant} (ΔC_{ant}) spatial variability and its effect on the acidification rates and other carbonate system properties in the South Atlantic Ocean over the last 30 years (1989–2019), using a slightly modified version of the ensemble eMLR approach developed recently (e.g., Carter et al., 2017; Clement & Gruber, 2018). Additionally, we also evaluated the changes in the carbonate system variables due to the remineralization of organic matter. Although we analyzed the entire water column below the mixed layer, our focus was on the ocean's upper 2000 m.

2. Data and Methods

2.1. Data Selection

Data from 14 cruises along five hydrographic sections in the South Atlantic Ocean (Figure 1, Table S1 in Supporting Information S1) were extracted from the Global Ocean Data Analysis Project version 2 (GLODAPv2.2021; Lauvset et al., 2021) and analyzed. Between 1989 and 2021, three of these hydrographic sections were occupied three times in total (A10, A16, and A17), while the remaining sections (A9.5 and A13/A13.5) were occupied only two times. By extracting the data from the GLODAPv2.2021 rather than using the original cruise data, we benefit from the applied adjustment of the properties that makes all data internally consistent. Thus, further corrections were not applied.

Except for the A13/A13.5 section, the station positions between occupations were consistent, with less than 50 nautical miles of variation between repetitions. For the A13/A13.5 section, the distances between the stations of the first (A13) and second (A13.5) occupation were greater and varied from ~250 nm at 10°S to ~400 nm at 40°S. This difference results from the utilization of data from the A13.5 section in the analysis, and this was necessary due to the low number of observations in the eastern South Atlantic. Although it was assumed that both sections (A13 and A13.5) have similar dynamics, more care should be taken when interpreting these results, since, unlike the remaining sections, the differences observed here may also be influenced by the distance between stations. For simplicity, this section is referred to only as A13 hereafter.

An additional section (A10.5) was analyzed using data from the Brazilian Trans-Atlantic II (TAII) and the 06M220170104 cruises. However, the C_{ant} accumulation rates and inventories observed in this section were

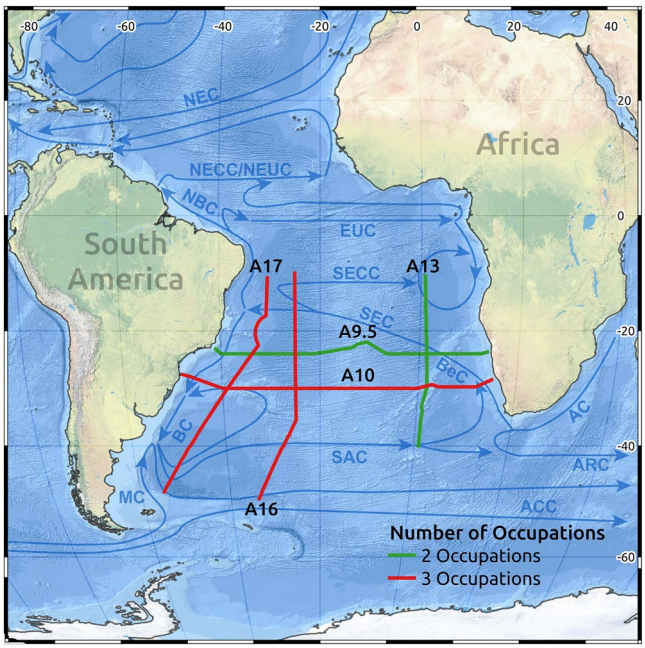

Figure 1. Map of the study region in the South Atlantic Ocean. The colored lines depict the position of the five Global Ocean Ship-based Hydrographic Investigations Program (GO-SHIP) hydrographic sections used in this work, and their color represents the number of occupations: green for two occupations (A9.5 and A13 sections) and red for three occupations (A10, A16, and A17 sections). Note that the A13 section shows the 33RO20100308 cruise, which corresponds to the GO-SHIP A13.5 section. The blue arrows represent the main upper-ocean currents in the South and Tropical Atlantic (Koszalka & Stramma, 2019). The ocean currents described are: Agulhas Current (AC), Agulhas Return Current (ARC), Antarctic Circumpolar Current (ACC), Benguela Current (BeC), Brazil Current (BC), Equatorial Undercurrent (EUC), Malvinas Current (MC), North Brazil Current (NBC), North Equatorial Current (NEC), North Equatorial Countercurrent (NECC), North Equatorial Undercurrent (NEUC), South Atlantic Current (SAC), South Equatorial Current (SEC) and South Equatorial Countercurrent (SECC).

unrealistic (i.e., values higher than expected when considering the carbonate chemistry and higher than those observed at similar latitudes in the meridional sections). This overestimation was attributed to the use of reconstructed carbonate system parameters for the earlier occupation (cruise TAII) and, to a lesser degree, to the low quantity of parameters used in these regressions. Thus, these results were not included in the main text (but can be found in the Supporting Information S1).

2.2. Water Masses Identification

Our analysis considered the full depth of the water column below the surface mixed layer (~150 m, Holte et al., 2017). However, the central and intermediate waters were the focus of this study, as significant decadal C_{ant} changes have been observed mainly in these waters (Wanninkhof et al., 2010; Woosley et al., 2016). Guided by earlier water mass definitions (Hernández-Guerra et al., 2019; Manta et al., 2021; Stramma & England, 1999) the first 1100 m of the water column were split into two layers (hereafter referred to as central and intermediate water layers) using the neutral density (γ^n) values extracted from the GLODAPv2-2021 database (calculated following Jackett & McDougall, 1997). The central water layer was defined by γ^n boundaries between 26.2 kg m^{-3} and 27.1 kg m^{-3}, which goes from ~150 to ~750 m, and is mainly composed of the South Atlantic Central Water (SACW). The SACW is formed by subduction along the subtropical gyre of the South Atlantic Ocean, north of the Subtropical Front, being ventilated mainly by three varieties of Subtropical Mode Water (STMW) (Gordon, 1981; Provost et al., 1999; Sato & Polito, 2014). In the western margin, the lower layer of the SACW (γ^n > 26.5 kg m^{-3}) is influenced by the Subantarctic Mode Water (SAMW), formed by subduction at the north of the Subantarctic Front during the winter (Mémery et al., 2000; Tanhua et al., 2017). The intermediate water layer was defined by 27.1 kg m^{-3} < γ^n < 27.65 kg m^{-3}, which covers the depth range from ~750 to ~1100 m, and is composed of the Antarctic Intermediate Water (AAIW). Both layers are influenced by water masses entering the South Atlantic from the Indian Ocean via the Agulhas Retroflection (Azar et al., 2021; de Souza et al., 2018; Poole & Tomczak, 1999). For a more detailed description of the water masses in the studied region, see Stramma and England (1999) and Hernández-Guerra et al. (2019).

2.3. Change in Hydrographic Properties and ΔC_{org}

The change in the hydrographic properties (e.g., salinity, apparent oxygen utilization -AOU-, dissolved inorganic carbon -DIC-, total alkalinity -Alk- and nitrate) between occupations was calculated for every section. Data were gridded in a 0.5° by 0.05 kg m^{-3} grid with an objective interpolation scheme (Barnes interpolation) using the *oce* package for R (Kelley & Richards, 2022). Neutral density was used as the z-coordinate instead of depth to eliminate part of the variability associated with mesoscale activity and to allow a direct comparison of the results with previous studies (e.g., Fine et al., 2017). For the Barnes interpolation, a total of two iterations and a smoothing parameter of 0.2 were used, following the algorithm and recommendations of Koch et al. (1983). To avoid spurious interpretations in not sampled areas, the interpolated values were trimmed in the regions where the data weights were lower than the 0.3 percentile. The uncertainties introduced by the interpolation were calculated by direct comparison of the measured and interpolated values, and the root mean square errors (RMSEs) were estimated for the different water layers and for the entire water column (Table S3 in Supporting Information S1).

The dissolved inorganic carbon (DIC) changes caused by the remineralization of organic matter (ΔC_{org}) were derived from the gridded variations in the apparent oxygen utilization (AOU) and the remineralization ratio ($r_{c:o}$ = 117/170) of Anderson and Sarmiento (1994) following Equation 1:

$$\Delta C_{org} = r_{c:o} \times \Delta AOU \quad (1)$$

For a direct comparison with the ΔC_{ant} estimates, the gridded ΔC_{org} values were interpolated to the position of the samples collected in the most recent occupation through a pointwise bivariate interpolation scheme using the *akima* package for R (Akima & Gebhardt, 2022).

2.4. Anthropogenic Carbon Calculations

The quantification of the oceanic C_{ant} uptake dates back to the end of the 1970s (e.g., Brewer, 1978; Chen & Millero, 1979; for a historical review see Sabine & Tanhua, 2010). One approach frequently used consists in the determination and decomposition of DIC changes into a part that can be associated with natural processes, tightly linked with variations in other biogeochemical and physical variables (Zeebe & Wolf-Gladrow, 2001) and a residual that is interpreted as the ΔC_{ant}. Multiple methods that use this principle have been developed, such as those that depend on quasi-conservative tracers (e.g., Gruber et al., 1996; Touratier & Goyet, 2004) or multiple linear regressions (e.g., Friis et al., 2005; Wallace, 1995). The extended multiple linear regression method (eMLR) developed by Friis et al. (2005) has become one of the most popular methods to estimate the C_{ant} uptake from repeated hydrographic sections data (e.g., Carter et al., 2017; Salt et al., 2015; Tanhua et al., 2017; Wanninkhof et al., 2010; Waters et al., 2011; Williams et al., 2015; Woosley et al., 2016).

The eMLR method makes two assumptions: (a) the multiple linear regressions can describe the natural distribution of the DIC, that is, the physical and biogeochemical variables have a linear relationship with the natural variability in DIC, and (b) the ocean is in a steady-state, meaning that the correlation between the DIC and the independent variables do not change with time. Thus, the DIC in both occupations is fitted individually following Equations 2 and 3:

$$DIC_{t1} = a_1 + b_1 V1_{t1} + c_1 V2_{t1} + \ldots + n_1 Vn_{t1} \quad (2)$$

$$DIC_{t2} = a_2 + b_2 V1_{t2} + c_2 V2_{t2} + \ldots + n_2 Vn_{t2} \quad (3)$$

where the subscript $t1$ and $t2$ indicate the first and the last occupation, a_1 to n_1 and a_2 to n_2 represent the coefficients of the first and the second regression respectively, and $V1$ to Vn represent the physical and biogeochemical parameters that are used to describe the spatial distribution of the DIC.

The C_{ant} uptake between the two cruises (ΔC_{ant}) is then calculated by subtracting the coefficients from Equation 1 and Equation 2 and using the values of the parameters at $t2$, as shown in Equation 4:

$$\Delta C_{ant} = (a_2 - a_1) + (b_2 - b_1) V1_{t2} + (c_2 - c_1) V2_{t2} + \ldots + (n_2 - n_1) Vn_{t2} \quad (4)$$

Although the original eMLR method has proven to be powerful identifying the ΔC_{ant} along repeated surveys (Goodkin et al., 2011; Levine et al., 2008), methodological modifications have improved the ΔC_{ant} determination, even from data that are not along repeat cruise lines (Clement & Gruber, 2018). For example, the eMLR is now usually applied along isopycnal surfaces because this is the preferential pathway of water masses movement and penetration of C_{ant} into the ocean (Gruber et al., 1996; Sabine et al., 2004; Wanninkhof et al., 2010) and because this allowed more robust fits (Clement & Gruber, 2018; Tanhua et al., 2017). More recently, Clement and Gruber (2018) developed a new method capable of estimate the ΔC_{ant} for the global ocean through the addition of a probabilistic method for the selection of predictors and the inclusion of C^* (defined as the DIC corrected by the remineralization of organic matter and the calcium carbonate dissolution, see Gruber et al., 1996) rather than DIC in the linear regressions. This method was used to quantify the global oceanic sink of C_{ant} over the period from 1994 to 2007 (Gruber, Clement, et al., 2019). Similarly, modifications proposed by Carter et al. (2017, 2019) allowed further refinement of the C_{ant} accumulation rates in the Pacific Ocean, which showed a lower bias and RMSEs compared to the Friis et al. (2005) method.

Here, the ΔC_{ant} below the surface mixed layer (depth >150 m) was quantified for the studied sections using the eMLR method with some of these modifications, including the utilization of the DIC corrected by the dissolution of organic matter (DIC_{abio}) instead of DIC in the multiple linear regressions, the employment of potential temperature (θ), salinity, AOU, Alk, Si, and NO_3^- as the independent variables in the 42 MLRs, and the utilization of the mean C_{ant} value derived from the 10 best regressions (quantified by the lower combined RMSE) as the final ΔC_{ant} estimate. For a full description of the modifications to the approach used here, see Text S1 in Supporting Information S1. Considering these modifications, and the fact that the average time between surveys occupations was approximately 10 years, a robust estimation of the C_{ant} in the South Atlantic Ocean was obtained, with uncertainties of ± 3 μmol kg^{-1} (see Text S2 in Supporting Information S1).

2.5. Changes in the Carbonate System Properties

The changes in pH and other carbonate system parameters due to organic matter remineralization and C_{ant} uptake were estimated directly from ΔC_{org} and ΔC_{ant} using Equations 5 and 6 proposed by Lauvset et al. (2020):

$$\Delta pH_{org} = pH^{f(DIC,\,Alk)} - pH^{f\left(DIC-\Delta C_{org},\,Alk-\mathrm{Alk}_{org}\right)} \tag{5}$$

$$\Delta pH_{ant} = pH^{f(DIC,\,Alk)} - pH^{f\left(DIC-\Delta C_{ant},\,Alk\right)} \tag{6}$$

where $pH^{f(DIC,\ Alk)}$ is the pH derived from the DIC and Alk values of the most recent occupation and Alk_{org} corresponds to the alkalinity changes steaming from the organic matter remineralization. This last term was calculated from the grided changes in AOU, the stoichiometric N:O ratio of Anderson and Sarmiento (1994) ($r_{n:o}$ = 16/170), and a coefficient that represent the influence of the nutrients remineralization over the Alk (−1.36) of Wolf-Gladrow et al. (2007) following Equation 7:

$$Alk_{org} = -1.36 \times r_{n:o} \times \Delta AOU \tag{7}$$

The organic matter remineralization was the only natural process taken into consideration since it is the most important natural component that explains the gradients of pH inside the oceans, and because the dissolution of calcium carbonate only has a significant influence below the intermediate waters (Lauvset et al., 2020). The carbonate system calculations were performed using the *carb* function of the *seacarb* package for R (Gattuso et al., 2020), with the K1 and K2 constant of Lueker et al. (2000), the Kf constant of Perez and Fraga (1987), the sulfate constant of Dickson (1990) and the borate constant of Lee et al. (2010), following the suggestions of Woosley (2021). The uncertainties of the carbonate parameters were propagated considering the equilibrium constants uncertainties of Orr et al. (2018) and the errors of each variable, using the equations of Lauvset et al. (2020). All the pH values reported in this work are in the total scale.

3. Results

3.1. DIC, AOU and ΔC_{org} in the South Atlantic Ocean

Multiple variations in the distribution of DIC were found throughout the water column in all sections studied (Figure 2). The central and intermediate layers were marked by a significant increase (>0.6 μmol kg^{-1} yr^{-1}) in the DIC concentrations and the highest changes (>±2 μmol kg^{-1} yr^{-1}) were observed in patches located above the intermediate waters. In contrast, the DIC changes in the deep and bottom waters were generally more modest (~±0.3 μmol kg^{-1} yr^{-1}), except for a large decrease (−2 μmol kg^{-1} yr^{-1}) observed in the AABW in the A13 section (Figure 2d) and the NADW between 2013 and 2019 in the A17 section (Figure 2c). In the central waters of the zonal sections (A9.5 and A10), the patches with the highest DIC changes were more abundant in the easter margin, between 0 and 10°E. In the meridional sections, only the A13 section showed a clear difference in the distribution of the DIC changes, with more positive changes in the central and intermediate waters south of 22°S. In those sections with more than two occupations (A10 and A16), a higher DIC increase was observed in the central waters during the 2000s–2010s compared with the earliest decade (Figures 2a and 2b). However, this trend was less evident in the A17 section (Figure 2c), where the DIC changes during the second period were less uniform than those observed between 1994 and 2013.

Compared with DIC, the AOU changes were smaller and presented a patchier distribution (Figure 3). The vertical distribution of AOU changes was similar to that observed for DIC, with the highest variations in the central and intermediate waters and few in the deep-water masses. In the zonal sections (A9.5 and A10), higher changes were found in the eastern margin (around 10°E) in comparison with the western margin (Figures 3a–3d). However, while the central waters in the A10 section were marked by negative AOU changes in all periods, positive values were observed in the A9.5 section between 20°W and 12°E. In the meridional sections, the highest changes were located in the tropical region (north of 20°S) and around the subtropical front (40°S), and the most common variation was an increase in the AOU values along the AAIW from 50°S to 30°S in almost every studied period.

In terms of distribution, the highest DIC changes observed as patches in the central and intermediate waters (Figure 2) were strongly correlated with the changes in AOU (Figure 3) and nutrients (Figure S9 in Supporting Information S1). Thus, it is not surprising that the highest ΔC_{org} changes (Figure 4), calculated from the AOU variations, coincided with the position of these largest DIC changes. However, the general increase in DIC

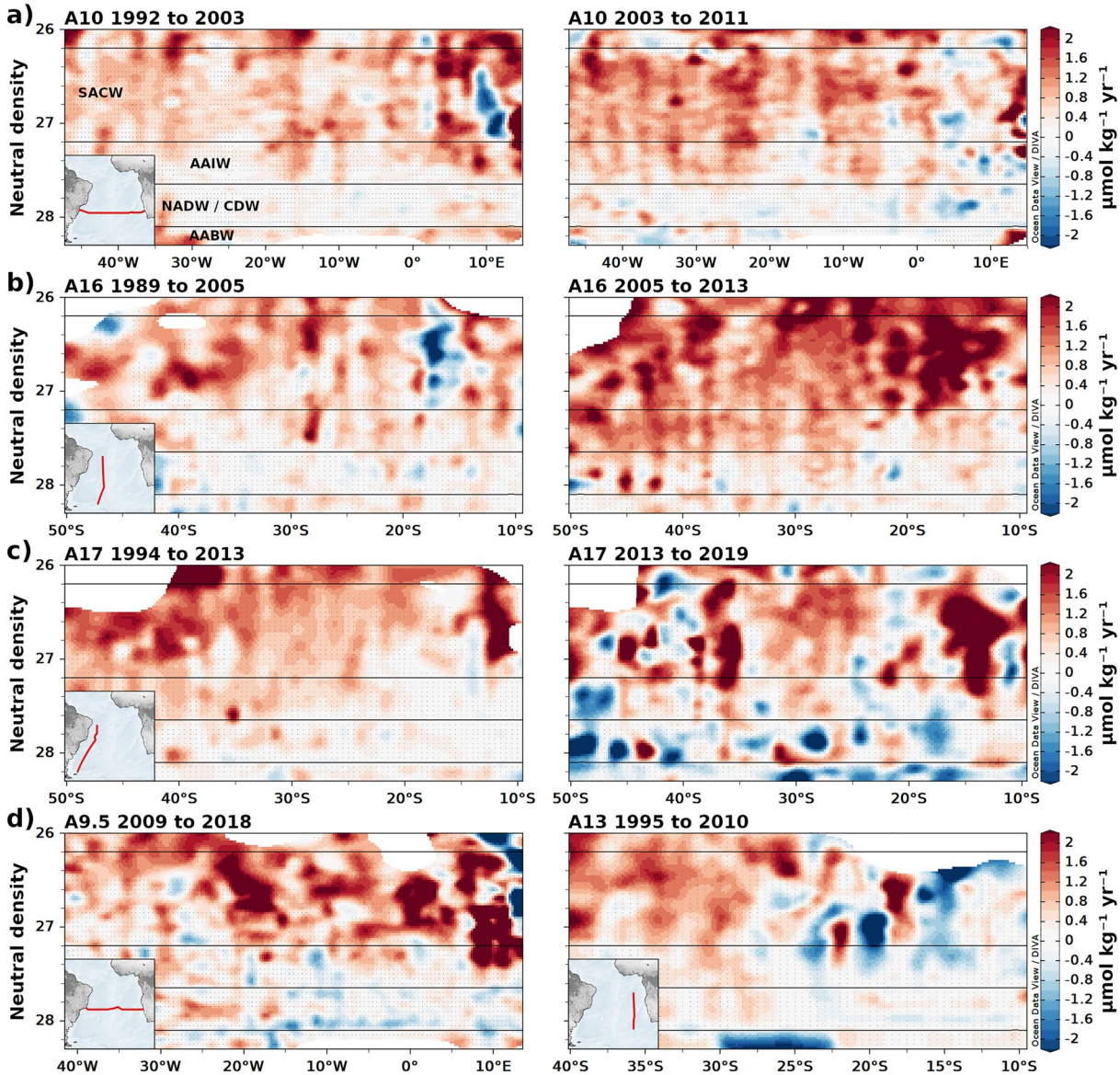

Figure 2. Dissolved inorganic carbon (DIC) variations observed in the central, intermediate a deep water masses of the South Atlantic Ocean for the sections occupied (a–c) three and (d) two times evaluated in this study. Positive (negative) values in red (blue) represent an increase (decrease) since the beginning of the period. The name of the sections and the years of sampling are shown in the panel title. Acronyms in the first panel stand for: South Atlantic Central Water (SACW), Antarctic Intermediate Water (AAIW), North Atlantic Deep Water (NADW), Circumpolar Deep Water (CDW), and Antarctic Bottom Water (AABW). Horizontal black lines depict (from top to bottom) the neutral density boundary of 26.2 kg m^{-3}, 27.2 kg m^{-3}, 27.65 kg m^{-3}, and 28.15 kg m^{-3}. The position of each section is indicated on the inset map.

observed in the central waters (Figure 2) is absent in the ΔC_{org} distribution (Figure 4). In contrast, in the AAIW, the ΔC_{org} more closely resembled the observed DIC changes, especially between 50°S and 30°S (Figures 4b and 4c). Over the studied region, the eastern basin north of 25°S (A9.5 section) was the zone with the most intense variations (Figure 4a), with ΔC_{org} highest than 3 µmol kg^{-1} yr^{-1}.

3.2. ΔC_{ant} Distribution and Accumulation Rates

A similar vertical distribution of ΔC_{ant} was found in all zonal and meridional sections along the South Atlantic Ocean, with statistically significant concentrations of C_{ant} down to 1000 m and small changes (not significant in most cases) in deep and bottom waters (Figure 5). The mean C_{ant} accumulation rate was three-fold higher in the central waters than in the intermediate waters, with values of 0.89 ± 0.33 µmol kg^{-1} yr^{-1} and

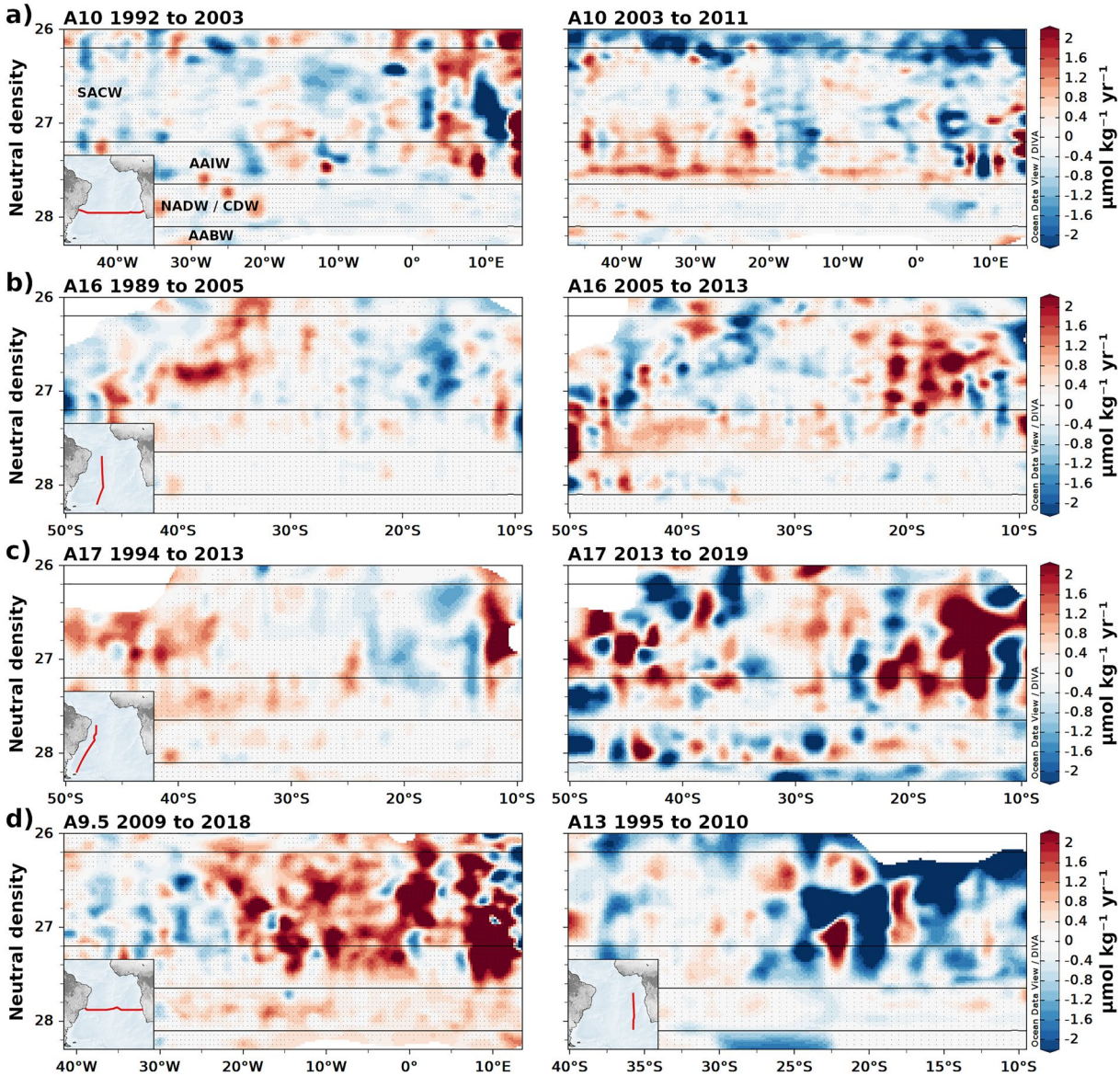

Figure 3. Apparent Oxygen Utilization (AOU) variations observed in the central, intermediate a deep water masses of the South Atlantic Ocean for the sections occupied (a–c) three and (d) two times evaluated in this study. Positive (negative) values in red (blue) represent an increase (decrease) since the beginning of the period. The name of the sections and the years of sampling are shown in the panel title. Acronyms in the first panel stand for: South Atlantic Central Water (SACW), Antarctic Intermediate Water (AAIW), North Atlantic Deep Water (NADW), Circumpolar Deep Water (CDW), and Antarctic Bottom Water (AABW). Horizontal black lines depict (from top to bottom) the neutral density boundary of 26.2 kg m^{-3}, 27.2 kg m^{-3}, 27.65 kg m^{-3}, and 28.15 kg m^{-3}. The position of each section is indicated on the inset map.

0.30 ± 0.29 µmol kg^{-1} yr^{-1}, respectively. Compared with the ΔC_{org} (Figure 4), the ΔC_{ant} distribution in the central waters was lest patchy, resembling more closely the total DIC changes observed in the region (Figure 2). However, the C_{ant} accumulation rates showed high spatial variability. For example, all the zonal sections presented a deeper C_{ant} penetration in the western basin than in the eastern basin. In the meridional sections, higher ΔC_{ant} were observed southward. In the intermediate waters of the A13 section, the ΔC_{ant} were observed up to 23°S, while in the remaining meridional sections the C_{ant} invasion reached lower latitudes.

The ΔC_{ant} spatial variability was more evident in the central waters, with increasing values southward and westward (Figure 6). The differences in C_{ant} accumulation rates between the south and north (~0.50 µmol kg^{-1} yr^{-1}) were two-fold higher than the east-west differences (~0.25 µmol kg^{-1} yr^{-1}), indicating a higher meridional gradient. In general, for those sections with three occupations (A10, A16, and A17), the accumulation rates

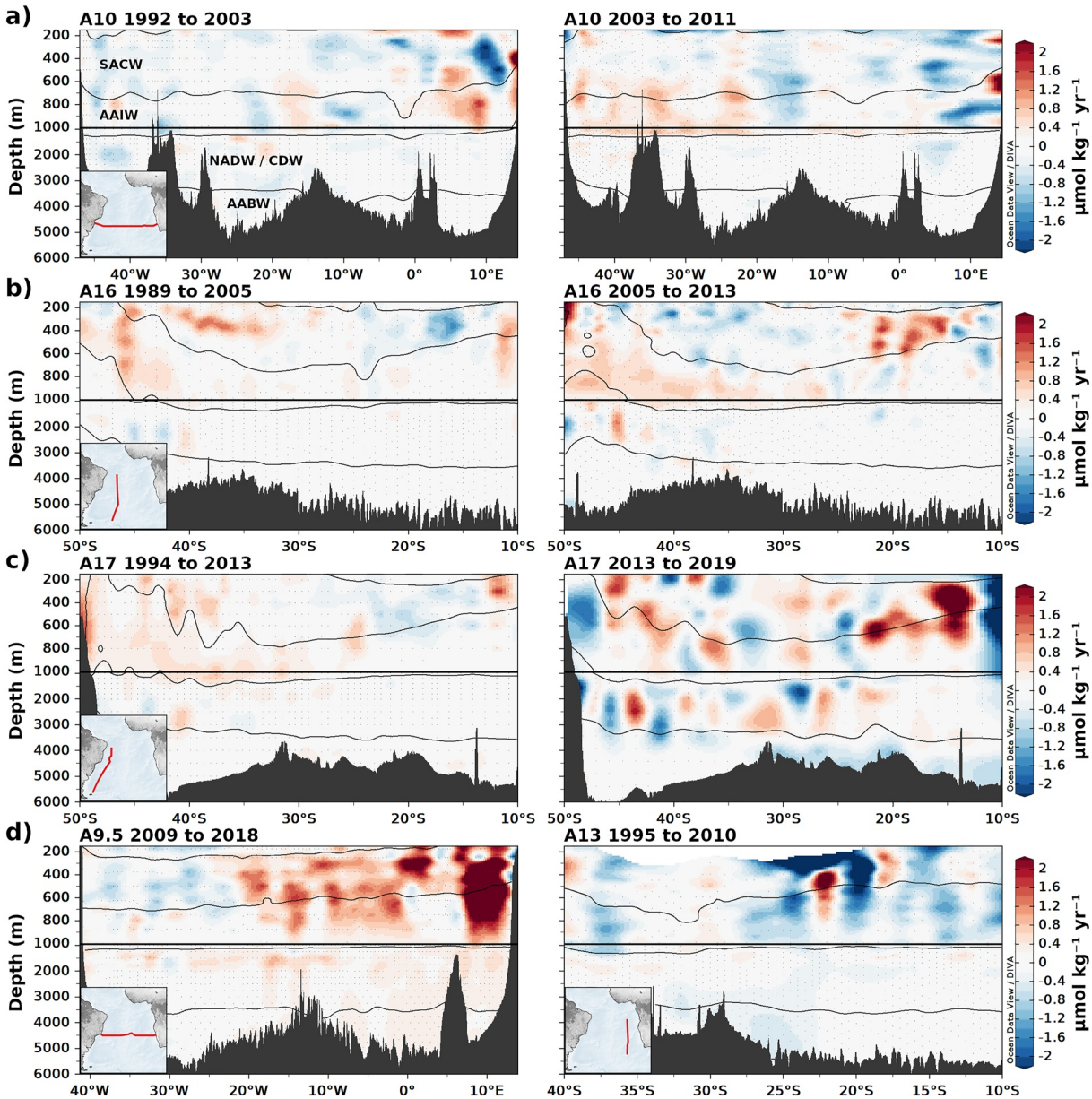

Figure 4. Annual changes in the dissolved inorganic carbon caused by the remineralization of organic matter (ΔC_{org}) for the sections occupied (a–c) three and (d) two times evaluated in this study. Positive (negative) values in red (blue) represent an increase (decrease) since the beginning of the period. The name of the sections and the years of sampling are shown in the panel title. Acronyms in the first panel stand for: South Atlantic Central Water (SACW), Antarctic Intermediate Water (AAIW), North Atlantic Deep Water (NADW), Circumpolar Deep Water (CDW), and Antarctic Bottom Water (AABW). Black lines depict (from top to bottom) the neutral density boundaries of 26.2 kg m^{-3}, 27.2 kg m^{-3}, 27.65 kg m^{-3} and 28.15 kg m^{-3}. The position of each section is indicated on the inset map.

increased from the 1990s to the 2000s, following the trend observed in the DIC changes. For example, an increase in the accumulation rates of 0.16 µmol kg^{-1} yr^{-1} was observed between decades in the central waters of the A10 section, whilst this difference was even higher in the A16 section, with a value of 0.52 µmol kg^{-1} yr^{-1}. However, this pattern was not present in the intermediate waters of the A10 section (Figure 6b) and the central waters of the A17 section (Figure 6a), where the accumulation rates of the oldest decade were higher.

Considering only the anthropogenic changes calculated from the eMLR method, an average column inventory change of 0.77 ± 0.39 mol C m^{-2} yr^{-1} was found for the South Atlantic Ocean from 150 to 2000 m between 1989 and 2019. If the C_{ant} changes in the first 150 m are also considered (assuming that the increase in the partial pressure of CO_2 in the surface waters was proportional to the atmospheric change, see Text S3 in Supporting

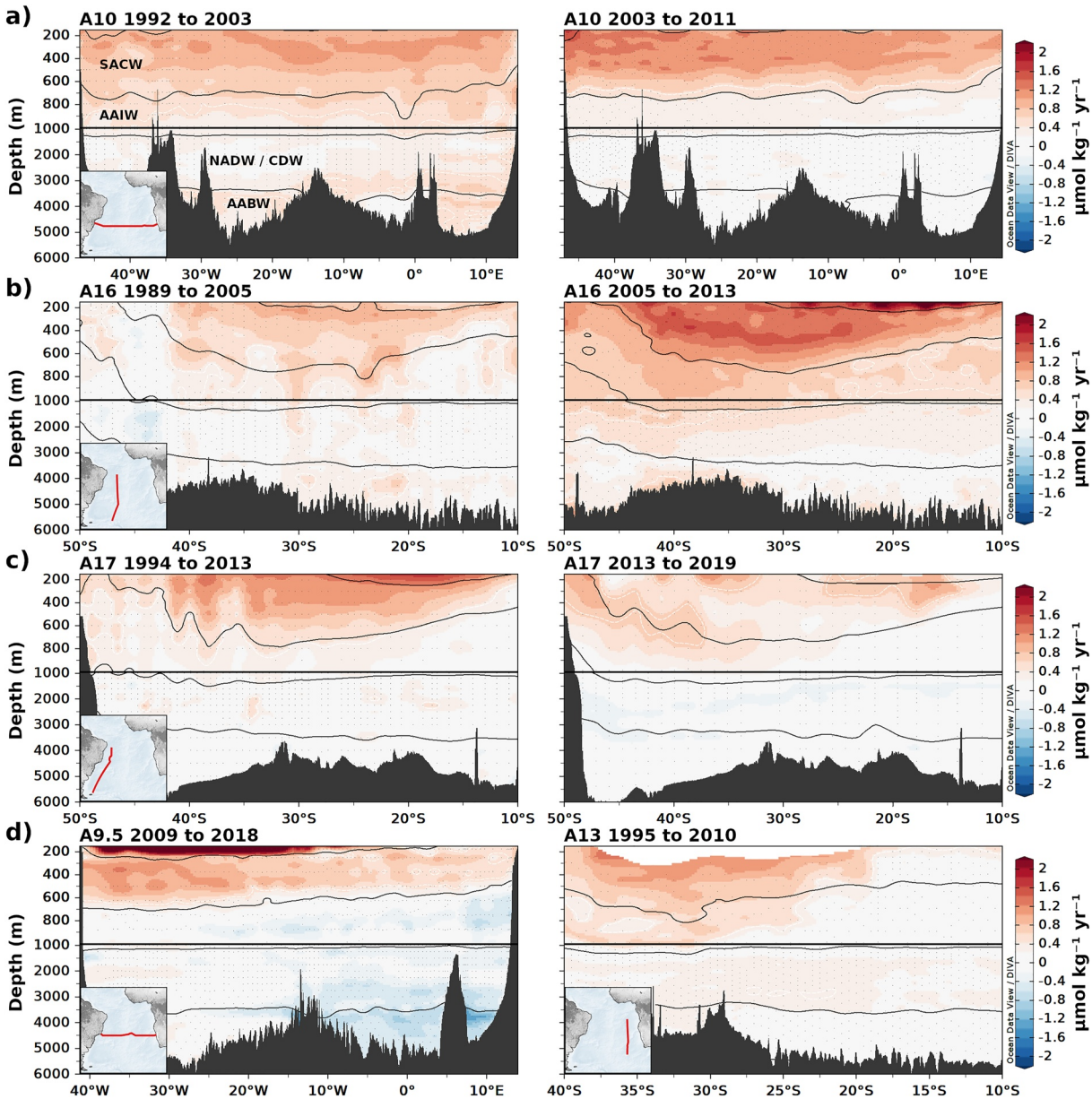

Figure 5. Annual changes in the dissolved inorganic carbon caused by the uptake of anthropogenic carbon (ΔC_{ant}) for the sections occupied (a–c) three and (d) two times evaluated in this study. Positive (negative) values in red (blue) represent an increase (decrease) since the beginning of the period. White dashed lines indicate the limit where ΔC_{ant} estimates are statistically distinguishable from 0 with a 90% confidence. The name of the sections and the years of sampling are shown in the panel title. Acronyms in the first panel stand for: South Atlantic Central Water, Antarctic Intermediate Water, North Atlantic Deep Water, Circumpolar Deep Water, and Antarctic Bottom Water. Black lines depict (from top to bottom) the neutral density of 26.2, 27.2, 27.65, and 28.15 kg m^{-3}. The position of each section is indicated on the inset map.

Information S1) the average column inventory change for the first 2000 m increases to 0.94 ± 0.39 mol C m^{-2} yr^{-1}. For each section, the inventory changes (Figure 6c) were consistent with the distribution patterns displayed by the accumulation rates, with higher meridional than zonal variations.

3.3. Changes in pH and Other Carbonate System Parameters

The DIC changes induced by both C_{ant} uptake and the remineralization of organic matter have driven the acidification of the South Atlantic Ocean upper waters. In general, the C_{ant} uptake was the main driver controlling the acidification observed in the central waters, while the organic matter remineralization plays a role in the acidification of the intermediate waters below the 27.2 kg m^{-3} isopycnal (Figure 7a). However, when the individual

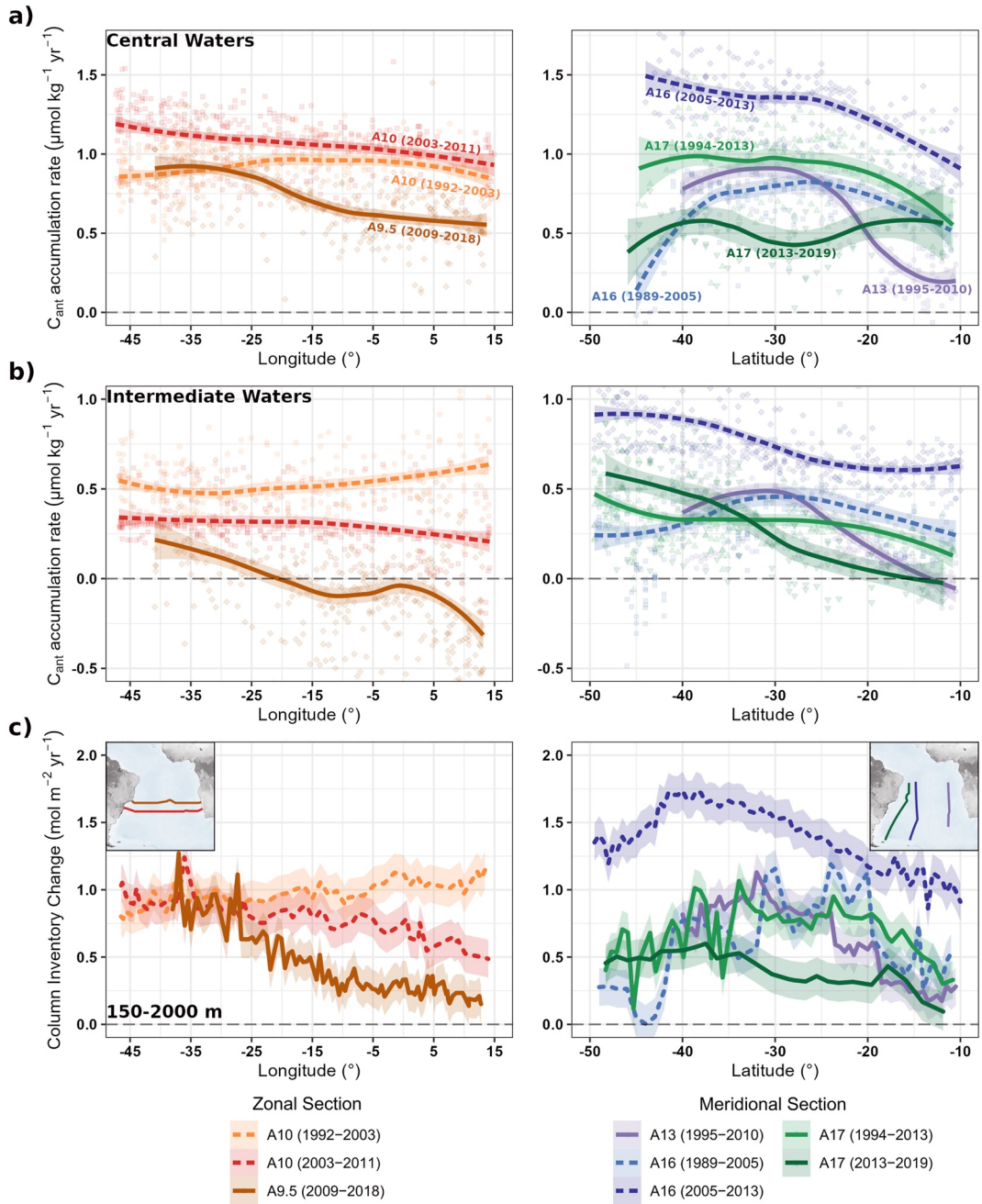

Figure 6. Annual (a–b) anthropogenic carbon (C_{ant}) accumulation rates and (c) column inventory changes between 150 and 2000 m in the zonal (left panels) and meridional (right panels) sections evaluated in this study. The dots represent the in situ data, while the lines show each section's results, and the colored shadows their uncertainties. Annual C_{ant} accumulation rates were calculated for the central ($\gamma^n < 27.2$ kg m^{-3}) and intermediate (27.2 kg m^{-3} < γ^n < 27.65 kg m^{-3}) waters. Column inventory changes were obtained by integration of the C_{ant} concentrations in each station from 150 to 2000 m and dividing the result by the number of years between each occupation, following the procedure described in Tanhua and Keeling (2012). The position of each section is indicated on the inset maps.

sections are studied, some patterns can be identified. For example, in the central waters, the influence of the organic matter remineralization over the pH changes increases from west to east in the zonal sections (Figure 7b) and for the meridional sections the organic matter remineralization has a more important role in the acidification of the waters south of 40°S and in the northern portion. Below the intermediate waters the pH changes were not statistically different from zero.

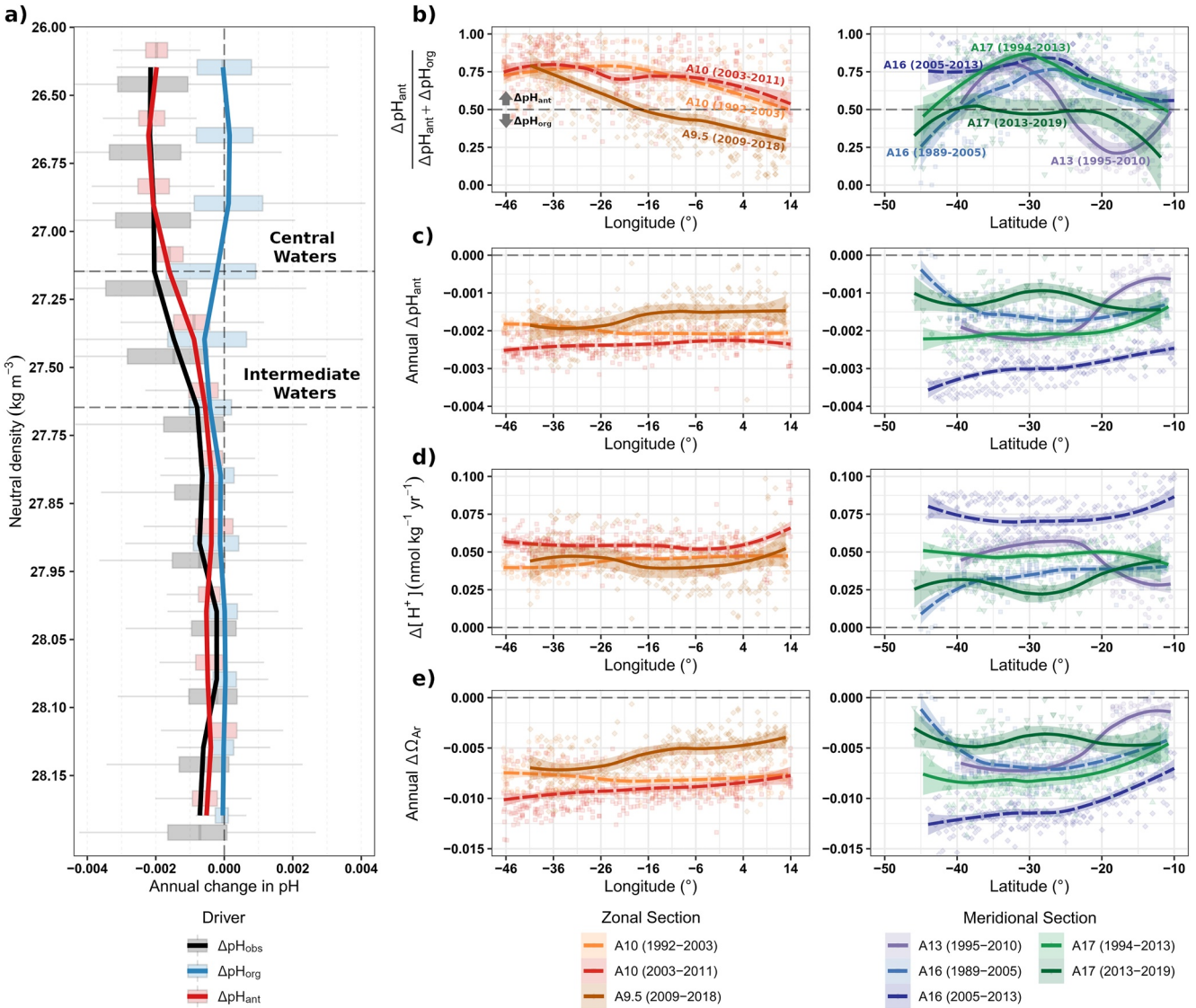

Figure 7. Changes in the carbonate system parameters in the South Atlantic Ocean. (a) Vertical profile showing the average changes in pH in 12 intervals of neutral density along the water column directly observed (ΔpH_{obs}) and inferred from the anthropogenic uptake (ΔpH_{ant}) and organic matter remineralization (ΔpH_{org}) estimates. The boxplots show a summary of the data distribution in each interval. (b) Relationship between ΔpH_{ant} and ΔpH_{org} and (c) annual changes in the acidification rates (d) hydrogen ion concentration and (e) aragonite saturation state for the central waters of the zonal (left) and meridional (right) sections evaluated in this study due to the anthropogenic change. The dots represent the in-situ data, while the lines were obtained by local polynomial regression fitting. Uncertainties are shown by the colored shadows.

The C_{ant} acidification rates observed in the region were -0.0020 ± 0.0007 pH units yr^{-1} and -0.0009 ± 0.0009 pH units yr^{-1} for central (Figure 7c) and intermediate waters, respectively. Considering only the C_{ant} uptake in the central waters, the pH changes were accompanied by an increase in hydrogen ion concentration ([H$^+$], Figure 7d), along with a decrease in the aragonite saturation state (Figure 7e). The anthropogenic changes in the carbonate system properties showed the same distribution found for the C_{ant} content, with exception of the [H$^+$], where highest changes were observed in the eastern margin of the A9.5a and A10 sections and the northern end of the more recent occupation of the A16 section (Figure 7d).

4. Discussion

As observed in our results, the DIC variability (and consequently the changes in the carbonate system parameters) between occupations is a direct consequence of the anthropogenic perturbation (ΔC_{ant}) superimposed over a

natural signal (ΔC_{org}) that arises from changes in the organic matter remineralization in the ocean's interior (which also affect the AOU distribution), and this coincides with previous studies in the South Atlantic (Wanninkhof et al., 2010; Woosley et al., 2016). In the next section, we discuss the possible drivers behind the changes in the organic matter remineralization in the area. This is followed by an evaluation of the reconstructed ΔC_{ant} changes in this study, as significant bias in these estimates can impact the calculated acidification rates. We conclude with an identification of the areas most affected by ocean acidification and a discussion of the changes expected in the region in the coming years.

4.1. Drivers of the Remineralization Changes in the South Atlantic Ocean

The increased organic matter remineralization observed in the AAIW shows that this water mass is becoming less oxygenated, with a mean rate of AOU change of 0.23 ± 0.68 μmol kg^{-1} yr^{-1} south of 30°S. This estimate agrees well with the deoxygenation trend found by Santos et al. (2016) for the AAIW between 1960 and 2015 in the South Atlantic subtropical gyre (-0.18 ± 0.04 μmol kg^{-1} yr^{-1}) and the AOU rate of Fontela et al. (2021) in the Argentine Basin (0.38 ± 0.13 μmol kg^{-1} yr^{-1}). Furthermore, this result is in line with the observed AAIW deoxygenation found by Schmidtko et al. (2017) in the last two decades. Deoxygenation in the upper 1000 m of the ocean has been associated with warming-induced declines in oxygen solubility (Santos et al., 2016; Schmidtko et al., 2017). However, only circulation changes such as the reduced ventilation of the AAIW or an enhanced flux of organic matter can explain the increased remineralization inferred from AOU. While the direct identification of the main driver behind those changes is not possible with the available data, we can evaluate if the observed results are consistent with the variations identified in this region.

Ocean circulation changes on decadal scales have been identified previously in the area. Using the distribution of transient tracers and water age models, a decrease in the SAMW age and an increase in the Circumpolar Deep Water (CDW) age were observed along the South Atlantic Ocean (Fine et al., 2017; Tanhua et al., 2017; Waugh et al., 2013). The decrease in SAMW age, evidence of increased ventilation between the 1990s and 2000s, was attributed to the intensification and poleward displacement of westerly winds, which caused an intensification of the northward Ekman transport and increased STMW formation rates over the entire Southern Ocean (Gruber, Landschützer, et al., 2019; Waugh et al., 2013). The AOU decrease from 1989 to 2013 observed in the central waters in all sections except for the eastern part of the A9.5 section is coherent with the increased ventilation reported in the SAMW by earlier studies (Fine et al., 2017; Tanhua et al., 2017; Waugh et al., 2013). Furthermore, although no conclusive changes in AAIW ventilation north of 40°S have been previously inferred from transient tracer data, the increased remineralization observed in this study between the isopycnals of 27.2 and 27.65 kg m^{-3} in the meridional Sections A16 and A17 is in good agreement with the increased age of the waters observed south of 40°S (Tanhua et al., 2017; Waugh et al., 2013). Thus, circulation changes may explain not only the overall AOU patterns in the open ocean but also some of the interdecadal ΔC_{ant} variability observed in our study, as discussed below.

Although the consensus is that physical variations are the predominant mechanism of oxygen change in the oceans (Talley et al., 2016; Wanninkhof et al., 2010) and biological productivity is low in the subtropical gyres (Dunne et al., 2007), areas with positive trends in primary productivity have been observed in the last 20 years in South Atlantic gyre (Kulk et al., 2020). Therefore, some of the remineralization changes in our results may also be attributed to increased organic matter fluxes associated with enhanced productivity, especially in the eastern basin nearshore, where the highest phytoplankton biomass concentrations have been found (Carvalho et al., 2021). This is the case of the A9.5 section, where increased remineralization was observed east of 10°E around 500 m, in the domain of the Benguela Upwelling System. Primary productivity in the Benguela Upwelling System is controlled by the input of nutrient-rich waters coming from the Angola Gyre (Schmidt & Eggert, 2016). The strength of the upwelling favors a high interannual and decadal variability, associated with shifts in the magnitude and meridional position of the atmospheric South Atlantic Anticyclone (Lamont et al., 2018). Thus, more intense upwelling and primary productivity in 2018 could explain the increased remineralization observed here. The results of Lamont et al. (2018) also show that the upwelling in the Southern Benguela Upwelling System (south of 27°S) is an order of magnitude lower than in the north, which can explain the absence of changes of the same intensity in the east portion of the section A10.

Finally, it is important to highlight that one potential bias source in our analysis comes from the use of AOU as a proxy of organic matter respiration, as previous works have shown that water masses are not necessarily saturated

in oxygen during the subduction (Ito et al., 2004; Russell & Dickson, 2003). However, Carter et al. (2021) showed that the overestimation of organic matter remineralization that comes from the utilization of AOU in the thermocline of the subtropical gyre is small in comparison to the values observed in other regions, such as the Southern Ocean (south of 60°S) and the western North Pacific Ocean. Additionally, the nitrate changes in the sections (Figure S9 in Supporting Information S1) agree well with the ΔC_{org} found here.

4.2. Anthropogenic Carbon Changes in the South Atlantic Ocean

The C_{ant} inventory change of 0.94 ± 0.39 mol C m^{-2} yr^{-1} found here for the South Atlantic Ocean between 1989 and 2019 is higher (but within the uncertainty) than the mean global inventory change of 0.65 ± 0.08 mol C m^{-2} yr^{-1} found between 1994 and 2007 (Gruber, Clement, et al., 2019). This is expected, as our results show that a considerable amount of carbon is transported from the surface to the ocean's interior. The high C_{ant} inventory changes and accumulation rates observed in the region have been associated with lower Revelle factor values and a high volume of newly formed central and intermediate waters (Sabine et al., 2004). Additionally, our estimate includes the inventory changes of recent occupations outside the period studied by Gruber, Clement, et al. (2019) (e.g., A16 Section 2005-2013 or A9.5 Section 2009-2018) that are influenced by the increased atmospheric CO_2 growth rate observed in the last decade (Dlugokencky & Tans, 2022).

The main pattern found in the spatial distribution of C_{ant} in the South Atlantic Ocean was an increased concentration southward and westward, with a higher variation in the meridional sections in comparison with the zonal sections, except at 25°S (A9.5 section). This pattern can be explained by considering the differences in ventilation across the region, which depend on the circulation patterns and the distance to the water mass formation areas. Wallace (2001) concluded that the southward C_{ant} increase in the AAIW between 10°S and 30°S in the South Atlantic during the 1990s was observed because waters at the south were closest to their formation region and were ventilated more recently. Similarly, Murata et al. (2008) suggested that the formation of STMW in the confluence region between the Brazil and Malvinas Currents contributes to the ventilation of the central waters, resulting in an elevated C_{ant} signal in the western margin. Orselli et al. (2018) also pointed out that the higher C_{ant} in SACW and AAIW samples along the Patagonian shelf-break could be observed because these waters occupy a well-ventilated layer due to the proximity to their formation region. The water age estimates of Fine et al. (2017) at the isopycnal of 26.8 kg m^{-3} validate those observations, and the higher age difference observed longitudinally south of 30°S explains the higher variation in the C_{ant} content in the meridional sections. North of 30°S, older waters are found in the east as the influence of the eastern boundary shadow zone (Angola Dome) increases (Karstensen et al., 2008), explaining the highest zonal differences observed in the A9.5 section.

In terms of temporal changes, the increase in the C_{ant} accumulation rates from the 1990s–2000s to the 2000s–2010s observed in the central waters of the A10 and A16 sections is coherent with the higher atmospheric CO_2 growth rate during the last decades (Dlugokencky & Tans, 2022) and similar changes have been observed not only in the South Atlantic Ocean (Gao et al., 2022; Woosley et al., 2016) but also in other basins (e.g., Carter et al., 2019). Interestingly, larger C_{ant} column inventories changes are expected for the 2000s–2010s in comparison with the previous decade, but this is only true for the A16 section (Table 1). In the A10 section, the elevated accumulation rates observed in the intermediate waters between 1992 and 2003, particularly at the east of 10°E, resulted in the higher C_{ant} column inventory obtained during this period in comparison with the newest occupation (Figure 6c). While these higher accumulation rates in the intermediate waters between 1992 and 2003 could be attributed to a bias in our reconstruction of the C_{ant} in the A10 section, a similar signal has been observed not only by Woosley et al. (2016) but more recently by Gao et al. (2022) who reported that during 2003–2011 the ΔC_{ant} was confined within the surface and central waters in contrast with the behavior observed between 1992 and 2003. One plausible explanation is that changes in the circulation caused a reduction in the ventilation of the intermediate waters during the most recent decade and this is consistent with both, the increased AOU values along this water mass in our results (Figure 3) and the weaker upper-ocean circulation during the 2000s obtained by numerical model simulations (DeVries et al., 2017). However, it is difficult to explain how these circulation changes altered the C_{ant} uptake in the intermediate waters in the A10 section but not the A16 section. Another result that highlights the complex nature of the temporal changes is the low inventory change observed in the A17 section between 2013 and 2019, which cannot be explained by variations in the atmospheric forcing. While the accumulation rates in this section have a higher relative uncertainty due to the low time between occupations, more data is necessary to determine if these lower values are the result of interannual variability or if some other process is acting in this region.

Table 1
Anthropogenic Carbon Accumulation Rates and Column Inventories (0–2000 m) for the Atlantic Ocean

Section	Reference	Period	Method	Previous results	This study
Inventories (mol m^{-2} yr^{-1})					
A9.5		2009–2018	eMLR		0.64 ± 0.29
A10	Murata et al. (2008)	1992–2003	ΔnC_T^{CAL}	0.6 ± 0.1	1.13 ± 0.08
	Gao et al. (2022)	1992–2003	eMLR	0.99 ± 0.12	
	Woosley et al. (2016)	2003–2011	eMLR	0.83 ± 0.1	0.97 ± 0.14
	Gao et al. (2022)	2003–2011	eMLR	1.11 ± 0.22	
A13	Gao et al. (2022)	1983–2010	eMLR	0.57 ± 0.22	0.77 ± 0.29
A16	Wanninkhof et al. (2010)	1989–2005	eMLR	0.76 ± 0.2	0.75 ± 0.31
	Gao et al. (2022)	1989–2005	eMLR	0.76 ± 0.25	
	Gao et al. (2022)	2005–2013	eMLR	1.24 ± 0.37	1.56 ± 0.23
A17	Ríos et al. (2012)	1994–2013	φC_T^0	0.92 ± 0.13[b]	0.86 ± 0.21
		2013–2019	eMLR		0.60 ± 0.12
A7	Fajar et al. (2015)	1993–2010	φC_T^0	1.07 ± 0.23	
A16[a]	Wanninkhof et al. (2010)	1989–2003	eMLR	0.53 ± 0.05	
Accumulation Rates (μmol kg^{-1} yr^{-1})					
A9.5		2009–2018	eMLR		0.68 ± 0.38 (SACW)
					−0.05 ± 0.27 (AAIW)
A10	Murata et al. (2008)[c]	1992–2003	ΔnC_T^{CAL}	0.62 ± 0.15 (SAMW)	0.91 ± 0.15 (SACW)
				0.33 ± 0.13 (AAIW)	0.53 ± 0.15 (AAIW)
	Woosley et al. (2016)	2003–2011	eMLR	0.98 ± 0.17	1.08 ± 0.18 (SACW)
					0.30 ± 0.15 (AAIW)
A13		1995–2010	eMLR		0.59 ± 0.34 (SACW)
					0.26 ± 0.25 (AAIW)
A16		1989–2005	eMLR		0.75 ± 0.21 (SACW)
					0.37 ± 0.22 (SACW)
	Woosley et al. (2016)	2003–2011	eMLR	1.04 ± 0.28	1.28 ± 0.23 (SACW)
					0.64 ± 0.09 (AAIW)
A17	Ríos et al. (2015)[c]	1994–2013	φC_T^0	1.1 ± 0.1 (SACW)[a]	0.92 ± 0.24 (SACW)
				0.4 ± 0.2 (AAIW)[a]	0.31 ± 0.14 (SACW)
		2013–2019	eMLR		0.53 ± 0.23 (SACW)
					0.17 ± 0.19 (AAIW)
	Salt et al. (2015)	1994–2010	eMLR	0.99 ± 0.14 (SACW)	
				0.36 ± 0.06 (AAIW)	
A7	Fajar et al. (2015)	1993–2010	φC_T^0	0.96 ± 0.06 (SACW)	
				0.33 ± 0.06 (AAIW)	
A17	Ríos et al. (2015)[c]	1993–2003	φC_T^0	0.8 ± 0.2 (uNACW)	
				0.2 ± 0.1 (AAIW)	
Patagonian shelf-break	Orselli et al. (2018)[d]	Preindustrial-2008	TrOCA	0.35–0.66 (SACW)	
				0.11–0.41 (AAIW)	

Note. The acronyms represent the water masses: South Atlantic Central Water (SACW), Antarctic Intermediate Water (AAIW), Subantarctic Modal Water (SAMW) and Upper North Atlantic Central Water (uNACW), and South.

[a]From 64°N to 60°S. [b]Value obtained for the 1972–2003 period. [c]Values calculated by dividing the reported average C_{ant} concentrations by the elapsed time between each occupation. [d]Values calculated by dividing the reported average C_{ant} concentrations by the elapsed time since the Industrial Revolution and sampling period (~250–260 years).

At a regional scale, the accumulation rates and inventories reported here are in good agreement with previous results in the region (Table 1), which suggests that, in general, our methodology was able to capture the anthropogenic signal correctly. However, several observations must be made. Our column inventories changes in the A10 section are higher than previous estimates due to differences in the method used by Murata et al. (2008) for the C_{ant} determination for the early decade and the shallower integration used by Woosley et al. (2016) during 2003–2011. When our values are compared with the results of Gao et al. (2022), who used a similar methodology and integration depth, a better match is observed (excluding the difference in column inventories between decades in the A10 section discussed above). Another interesting contrast between our results and the previous studies is the lower (and not expected) anthropogenic uptake in the A16 section between 45°S and 42°S during 1989–2005, clearly visible in the column inventory changes (Figure 6d). The apparent lack of C_{ant} uptake is an artifact of the eMLR method and does not appear when we average the 42 MLR instead of the 10 best fits. While this is the only area where we observe a significant difference in the C_{ant} estimates across the entire water column due to the number of MLR averaged (Figure S3 in Supporting Information S1), this result highlight that caution should be taken during the selection of the regressions used in the ensemble variation of the eMLR method.

4.3. Acidification and Carbonate Changes in the South Atlantic Ocean

The uptake of C_{ant} was the main driver influencing the acidification up to 1100 m along the South Atlantic Ocean, accounting for approximately 90% and 50% of the pH changes observed in central and intermediate waters, respectively. The higher acidification rates associated with this process were found in the central waters, with a mean value of -0.0020 ± 0.0007 years^{-1} between 1989 and 2019. In general, the anthropogenic acidification rates in this study agree with previous results (Table 2). At 30°S (A10 section), our estimates of -0.0020 ± 0.003 years^{-1} and -0.0024 ± 0.003 years^{-1} in the central waters between 1993-2003 and 2003–2011 are similar to the values found by Woosley et al. (2016) for the first 250 m during the same periods. For the A16 section, higher estimates (but within the uncertainty) were found in comparison with Woosley et al. (2016). This can be partially explained by geographic differences, as their analysis included the North Atlantic Ocean which suffered a lower uptake of C_{ant} during the 1990s (Gruber et al., 2019; Wanninkhof et al., 2010), decreasing their estimate. However, as a higher C_{ant} uptake was observed in the North Atlantic Ocean in the 2000s, the difference between the most recent estimates cannot be attributed to the same effect, suggesting that our estimation of C_{ant} in this section during the 2005–2013 period may be somewhat overestimated.

The western basin is the most studied area of the South Atlantic Ocean, allowing the comparison of anthropogenic acidification rates up to the intermediate waters. Estimates of -0.0020 ± 0.0004 years^{-1} and -0.0009 ± 0.0004 years^{-1} in central and intermediate waters found in that region (A17 section) are similar to the previous values reported by Ríos et al. (2015) and Salt et al. (2015) (Table 2). These trends are also in agreement with those reported from the South Brazil Bight (Carvalho-Borges et al., 2018) to the Patagonian shelf-break (Orselli et al., 2018). In the Argentine basin, the acidification values reported by Fontela et al. (2021) are higher in the AAIW, because they represent the total change in pH observed in those waters and not the acidification rate associated only with the C_{ant} increase. However, as 60% of the pH change in the AAIW results from the C_{ant} uptake (Fontela et al., 2021), the approximated acidification rate in those waters of -0.0013 years^{-1} is in line with our findings. The relatively high acidification found in this region in comparison with the subtropical North Atlantic indicates that the South Atlantic Gyre is acidifying faster than its northern counterpart, a phenomenon also observed by Kitidis et al. (2017).

The remineralization of organic matter only has a considerable influence on the pH changes in the intermediate waters, but this effect is enough to make the total rates of acidification observed in this water mass similar to those observed at the surface (Figure 7) and even higher in the eastern basin nearshore Africa at 25°S, where the highest rates of acidification were found (Figure S5 and S6 in Supporting Information S1). This pattern of increased acidification in the intermediate waters in comparison with the upper layer was previously observed by Ríos et al. (2015) and Fontela et al. (2021) along the A17 section, but our results show that a similar feature can also be found along the eastern margin. However, as the available data in this region is scarce, and has a low temporal resolution, new observations are necessary to constrain this effect during the 2010s decade.

Even though the impacts of ΔC_{ant} and ΔC_{org} on the pH changes were evaluated, it is important to highlight that DIC and Alk variations associated with natural processes can alter the magnitude of the anthropogenic changes, and this effect is more visible in the $[H^+]$ changes. For example, based on the zonal differences in C_{ant}

Table 2
Acidification Rates in Surface/Central Waters and Intermediate Waters Over the Atlantic Ocean and Across the World

Reference	Section/position or ocean area	Period	Previous results		This study	
			ΔpH (Surface/CW)	ΔpH (IW)	ΔpH (Surface/CW)	ΔpH (IW)
			pH units yr^{-1}	pH units yr^{-1}	pH units yr^{-1}	pH units yr^{-1}
	Atlantic Ocean					
This study	A13 (10°–40°S)	1995–2010			−0.0015 ± 0.0007	−0.0008 ± 0.0007
This study	A9.5 (24°S)	2009–2018			−0.0016 ± 0.0010	−0.0002 ± 0.0008
This study	A17 (10°–40°S)	2013–2019			−0.0012 ± 0.0005	−0.0005 ± 0.0005
Woosley et al. (2016)	A10 (30°S)	1992–2003	−0.0020 ± 0.0003		−0.0020 ± 0.0003	−0.0015 ± 0.0004
Woosley et al. (2016)	A10 (30°S)	2003–2011	−0.0022 ± 0.0004		−0.0024 ± 0.0003	−0.0009 ± 0.0004
Woosley et al. (2016)	A16 (63°N–30°S)	1989–2005	−0.0011 ± 0.0005		−0.0016 ± 0.0004	−0.0010 ± 0.0006
Woosley et al. (2016)	A16 (63°N–30°S)	2005–2013	−0.0021 ± 0.0010		−0.0029 ± 0.0004	−0.0019 ± 0.0002
Ríos et al. (2015)	A17 (14°–50°S)	1994–2013	−0.0020 ± 0.0002[a]	−0.0009 ± 0.0005[a]	−0.0020 ± 0.0004	−0.0009 ± 0.0004
Ríos et al. (2015)	A17 (18°–36°N)	1993–2003	−0.0015 ± 0.0003[a]	−0.0004 ± 0.0004[a]		
Salt et al. (2015)	A17 (18°–23°S)	1994–2011	−0.0016	−0.0010		
Fontela et al. (2021)	A17 (30°–51°S)	1972–2019	−0.0019 ± 0.0001	−0.0022 ± 0.0002		
Kitidis et al. (2017)	AMT (15°–31°S)	1995–2013	−0.0019			
Kitidis et al. (2017)	AMT (25°–38°S)	1995–2013	−0.0009			
Orselli et al. (2018)	Patagonian shelf-break	Preindustrial-2007/2008	−0.0018	−0.0010		
Carvalho-Borges et al. (2018)	South Brazil Bight	Preindustrial-2014	−0.0017	−0.0010		
Vázquez-Rodríguez et al. (2012)	Ena basin	1981–2008	−0.0009 ± 0.0001	−0.0006 ± 0.0001		
Takahashi et al. (2014)	BATS	1983–2010	−0.0018 ± 0.0002			
Takahashi et al. (2014)	Drake (SAZ)	2002–2012	−0.0023 ± 0.0007			
	Other Oceans					
Williams et al. (2015)	South Pacific (P16s)	2005–2011	−0.0024 ± 0.0009			
Carter et al. (2017)	Pacific Ocean (60°N–60°S)	1994–2014	−0.0015[a]			
Xue et al. (2014)	Indian Ocean	1962–2012	−0.0016 ± 0.0001			

[a]Values calculated dividing the reported acidification rate by the elapsed time between each occupation.

observed in this study, higher acidification rates are expected in the west in comparison with the easter margin, and indeed this pattern was observed in the zonal sections (Figure 7c). However, as the pH in the eastern margin is naturally lower due to the intense organic matter remineralization associated with the Benguela Upwelling System, the anthropogenic perturbation results in higher $[H^+]$ changes compared with those observed in the west, especially in the A9.5 section (Figure 7d). This difference between the trends of pH and $[H^+]$ arises from the logarithmic definition of pH (Fassbender et al., 2021). Additionally, the organic matter remineralization increases the DIC and reduces the buffer capacity of the waters, allowing enhanced anthropogenic acidification (Lauvset et al., 2020; Salt et al., 2015), and this effect has been described previously in other coastal upwelling systems around the globe (Feely et al., 2018; Lachkar, 2014).

Because the C_{ant} concentrations are still increasing, the central and intermediate waters in the South Atlantic are very vulnerable not only to enhanced anthropogenic acidification but also to an aragonite unsaturation. To evaluate these changes in the future, we recalculate the trends based on the variation of atmospheric CO_2 between occupations (rather than time) and assuming that these trends remain constant and considering the atmospheric CO_2 projections of Meinshausen et al. (2020) we found that under the SSP2-4.5 the AAIW will become unsaturated

in aragonite in ~30 years (Figure S11 in Supporting Information S1), in line with the predictions of Fontela et al. (2021). This time will be even shorter along the African coast, where aragonite unsaturation is expected in the next 10–20 years (Figure S11 in Supporting Information S1). For the SACW, a total unsaturation with respect to aragonite only was observed for the emissions projected under the SSP5-8.5 in the year 2060, close to the estimates of Fontela et al. (2021) for the Argentine Basin. However, while useful, these projections do not take into account the possible changes that may occur in the biological pump and the ocean circulation, highlighting that a model-based projection such as the one carried out by Fransner et al. (2022) in the Nordic Seas is necessary for the South Atlantic.

5. Summary and Conclusions

In this study, we evaluated the C_{ant} distribution, accumulation rates, and its effect on the carbonate system of central and intermediate waters in the South Atlantic Ocean. This was achieved thanks to the availability of new data coming from recent hydrographic surveys embedded in the international GO-SHIP program in the region. Making use of the adjusted cruise data from the GLODAPv2.2021 database we applied a modified eMLR approach. The C_{ant} distribution was not spatially uniform, and higher values were observed in the southern and western margin of the subtropical gyre, where the waters are closest to their formation region. From 1989 to 2019, central and intermediate waters accumulated C_{ant} at a rate of 0.89 ± 0.33 and 0.30 ± 0.29 μmol kg^{-1} yr^{-1}, respectively. A column inventory change of 0.94 ± 0.39 mol C m^{-2} yr^{-1} was found from the surface down to 2000 m. This C_{ant} uptake was the major process responsible for the acidification of the upper part of the water column, and rates of -0.0020 ± 0.0007 and -0.0009 ± 0.0009 pH units yr^{-1} were observed in central and intermediate waters, respectively. Under these conditions, it is expected that the AAIW will become unsaturated in aragonite in ~30 years under the emissions projected in the SSP2-4.5, in line with previous previsions (e.g., Fontela et al., 2021; Salt et al., 2015).

In addition to the ΔC_{ant}, we studied the DIC changes associated with the organic matter remineralization that have occurred in the South Atlantic Ocean since the 1990s until now. The main features observed were a negative ΔC_{org} in the central waters, a positive ΔC_{org} concentration in intermediate waters along the southern limit of the subtropical gyre, and significant ΔC_{org} increases in the coast of Africa, north of 25°S. While these signals are coherent with some of the ventilation changes observed in the region, we cannot discard the effect of enhanced primary productivity, especially nearshore. These natural changes coupled with the C_{ant} effect were responsible for the higher acidification of the AAIW, a process previously reported in the western South Atlantic (Fontela et al., 2021; Ríos et al., 2015) but also observed here in the eastern region. Furthermore, an aragonite unsaturation on central waters along the eastern margin of the South Atlantic Ocean is expected in the next 10–20 years if the anthropogenic changes maintain the present trend. These results highlight the need for more extensive monitoring in the eastern margin of the South Atlantic, which will allow us to identify if the interannual variability is similar in both basins, and how much the ecosystems health, marine life, and societies will be affected by these changes.

Data Availability Statement

Data from the TAII cruise and the code used for the calculations is available at https://doi.org/10.5281/zenodo.5205938. The GLODAPv2.2021 data was published by Lauvset et al. (2021) and can be accessed at the GLODAP website (https://www.glodap.info/).

Acknowledgments
This study is part of the activities of the Brazilian High Latitude Oceanography Group (GOAL, www.goal.furg.br), the Brazilian Ocean Acidification Network (BrOA, www.broa.furg.br), and the CARBON Team research group (www.carbonteam.furg.br). This study was sponsored by the Brazilian National Council for Scientific and Technological Development (CNPq; Grant Nos. 443258/2019-8; 442628/2018-8), the Brazilian Improving Coordination of Higher Education Personnel (CAPES, Grant No. 23038.001421/2014-30), and was supported by the TRIATLAS project, which has received funding from the European Union's Horizon 2020 research and innovation programme under grant agreement No. 817578. The TAII cruise was sponsored by the CNPq Grant No. 558267/2009-2, with logistics supported by the Ministry of Science, Technology, Innovation, and Communication (MCTIC), the Brazilian Ministerial Secretary for the Resources of the Sea (SECIRM), and the Brazilian Navy. The authors also acknowledge the support of the Graduate Program in Oceanology from the CAPES Foundation. A. Piñango acknowledges his master's scholarship from CAPES process No. 88887.374157/2019-00. I. B. M. Orselli acknowledges her CNPq PDJ Grant No. 151130/2020-5. R. Kerr and Carlos A. E. Garcia acknowledge their CNPq researcher grants Nos. 304937/2018-5, 309978/2021-1 and 309932/2019-0, respectively. Johannes Karstensen acknowledges funding from the European Union's Horizon 2020 research and innovation programme under grant agreement No. 862626 (EuroSea). We would like to thank the supporters, collaborators, and scientists behind the Global Ocean Data Analysis Project (GLODAP). We are very grateful for the constructive comments provided by Nicolas Gruber and one anonymous reviewer, who helped to improve the manuscript substantially.

References

Akima, H., & Gebhardt, A. (2022). Akima: Interpolation of irregularly and regularly spaced data. Retrieved from https://CRAN.R-project.org/package=akima

Anderson, L. A., & Sarmiento, J. L. (1994). Redfield ratios of remineralization determined by nutrient data analysis. *Global Biogeochemical Cycles*, *8*(1), 65–80. https://doi.org/10.1029/93GB03318

Azar, E., Piñango, A., Wallner-Kersanach, M., & Kerr, R. (2021). Source waters contribution to the tropical Atlantic central layer: New insights on the Indo-Atlantic exchanges. *Deep Sea Research Part I: Oceanographic Research Papers*, *168*, 103450. https://doi.org/10.1016/j.dsr.2020.103450

Brewer, P. G. (1978). Direct observation of the oceanic CO_2 increase. *Geophysical Research Letters*, *5*(12), 997–1000. https://doi.org/10.1029/GL005i012p00997

Broecker, W. S. (1991). Keeping global change honest. *Global Biogeochemical Cycles*, *5*(3), 191–192. https://doi.org/10.1029/91GB01421

Carter, B. R., Feely, R. A., Lauvset, S. K., Olsen, A., De Vries, T., & Sonnerup, R. (2021). Preformed properties for marine organic matter and carbonate mineral cycling quantification. *Global Biogeochemical Cycles*, *35*(1), e2020GB006623. https://doi.org/10.1029/2020GB006623

Carter, B. R., Feely, R. A., Mecking, S., Cross, J. N., Macdonald, A. M., Siedlecki, S. A., et al. (2017). Two decades of Pacific anthropogenic carbon storage and ocean acidification along Global Ocean Ship-based Hydrographic Investigations Program sections P16 and P02. *Global Biogeochemical Cycles*, *31*(2), 306–327. https://doi.org/10.1002/2016GB005485

Carter, B. R., Feely, R. A., Wanninkhof, R., Kouketsu, S., Sonnerup, R. E., Pardo, P. C., et al. (2019). Pacific Anthropogenic carbon between 1991 and 2017. *Global Biogeochemical Cycles*, *33*(5), 2018GB006154. https://doi.org/10.1029/2018GB006154

Carvalho, A. C. O., Kerr, R., Mendes, C. R. B., Azevedo, J. L. L., & Tavano, V. M. (2021). Phytoplankton strengthen CO_2 uptake in the south Atlantic Ocean. *Progress in Oceanography*, *190*, 102476. https://doi.org/10.1016/j.pocean.2020.102476

Chen, C.-T. A. (1982). On the distribution of anthropogenic CO_2 in the Atlantic and southern oceans. *Deep-Sea Research, Part A: Oceanographic Research Papers*, *29*(5), 563–580. https://doi.org/10.1016/0198-0149(82)90076-0

Chen, C.-T. A., & Millero, F. J. (1979). Gradual increase of oceanic CO_2. *Nature*, *277*(5693), 205–206. https://doi.org/10.1038/277205a0

Clement, D., & Gruber, N. (2018). The eMLR(C*) method to determine decadal changes in the global ocean storage of anthropogenic CO_2. *Global Biogeochemical Cycles*, *32*(4), 654–679. https://doi.org/10.1002/2017GB005819

Cubasch, U., Wuebbles, D., Chen, D., Facchini, M. C., Frame, D., Mahowald, N., & Winther, J.-G. (2013). Introduction. In D. F. Stocker, D. Qin, G.-K. Plattner, M. Tignor, S. K. Allen, & J. Boschung (Eds.), *Climate change 2013: The physical science basis. Contribution of working group I to the fifth assessment report of the intergovernmental panel on climate change* (pp. 119–158). Cambridge University Press.

de Carvalho-Borges, M., Orselli, I. B. M., de Ferreira, M. L. C., & Kerr, R. (2018). Seawater acidification and anthropogenic carbon distribution on the continental shelf and slope of the western South Atlantic Ocean. *Journal of Marine Systems*, *187*, 62–81. https://doi.org/10.1016/j.jmarsys.2018.06.008

de Souza, A. G. Q., Kerr, R., & de Azevedo, J. L. (2018). On the influence of subtropical mode water on the South Atlantic Ocean. *Journal of Marine Systems*, *185*, 13–24. https://doi.org/10.1016/j.jmarsys.2018.04.006

De Vries, T., Holzer, M., & Primeau, F. (2017). Recent increase in oceanic carbon uptake driven by weaker upper-ocean overturning. *Nature*, *542*(7640), 215–218. https://doi.org/10.1038/nature21068

Dickson, A. G. (1990). Standard potential of the reaction: AgCl(s) + 1/2H 2 (g) = Ag(s) + HCl(aq), and the standard acidity constant of the ion HSO4- in synthetic sea water from 273.15 to 318.15 K. *The Journal of Chemical Thermodynamics*, *22*(2), 113–127. https://doi.org/10.1016/0021-9614(90)90074-z

Dlugokencky, E., & Tans, P. (2022). *Trends in atmospheric carbon dioxide*. National Oceanic and Atmospheric Administration. Retrieved from http://www.esrl.noaa.gov/gmd/ccgg/trends/global.html

Doney, S. C., Balch, W., Fabry, V., & Feely, R. A. (2009). Ocean acidification: A critical emerging problem for the ocean sciences. *Oceanography*, *22*(4), 16–25. https://doi.org/10.5670/oceanog.2009.93

Doney, S. C., Busch, D. S., Cooley, S. R., & Kroeker, K. J. (2020). The impacts of ocean acidification on marine ecosystems and reliant human communities. *Annual Review of Environment and Resources*, *45*(1), 83–112. https://doi.org/10.1146/annurev-environ-012320-083019

Doney, S. C., Fabry, V. J., Feely, R. A., & Kleypas, J. A. (2009). Ocean acidification: The other CO_2 problem. *Annual Review of Marine Science*, *1*(1), 169–192. https://doi.org/10.1146/annurev.marine.010908.163834

Dunne, J. P., Sarmiento, J. L., & Gnanadesikan, A. (2007). A synthesis of global particle export from the surface ocean and cycling through the ocean interior and on the seafloor. *Global Biogeochemical Cycles*, *21*(4). https://doi.org/10.1029/2006GB002907

Fajar, N. M., Guallart, E. F., Steinfeldt, R., Ríos, A. F., Pelegrí, J. L., Pelejero, C., et al. (2015). Anthropogenic CO_2 changes in the equatorial Atlantic Ocean. *Progress in Oceanography*, *134*, 256–270. https://doi.org/10.1016/j.pocean.2015.02.004

Fassbender, A. J., Orr, J. C., & Dickson, A. G. (2021). Technical note: Interpreting pH changes. *Biogeosciences*, *18*(4), 1407–1415. https://doi.org/10.5194/bg-18-1407-2021

Feely, R. A., Doney, S. C., & Cooley, S. (2009). Ocean acidification: Present conditions and future changes in a high-CO_2 world. *Oceanography*, *22*(4), 36–47. https://doi.org/10.5670/oceanog.2009.95

Feely, R. A., Okazaki, R. R., Cai, W.-J., Bednaršek, N., Alin, S. R., Byrne, R. H., & Fassbender, A. (2018). The combined effects of acidification and hypoxia on pH and aragonite saturation in the coastal waters of the California current ecosystem and the northern Gulf of Mexico. *Continental Shelf Research*, *152*, 50–60. https://doi.org/10.1016/j.csr.2017.11.002

Fine, R. A., Peacock, S., Maltrud, M. E., & Bryan, F. O. (2017). A new look at ocean ventilation time scales and their uncertainties. *Journal of Geophysical Research: Oceans*, *122*(5), 3771–3798. https://doi.org/10.1002/2016JC012529

Fontela, M., Velo, A., Gilcoto, M., & Pérez, F. F. (2021). Anthropogenic CO2 and ocean acidification in Argentine Basin Water Masses over almost five decades of observations. *Science of the Total Environment*, *779*, 146570. https://doi.org/10.1016/j.scitotenv.2021.146570

Fransner, F., Fröb, F., Tjiputra, J., Goris, N., Lauvset, S. K., Skjelvan, I., et al. (2022). Acidification of the nordic seas. *Biogeosciences*, *19*(3), 979–1012. https://doi.org/10.5194/bg-19-979-2022

Friedlingstein, P., O'Sullivan, M., Jones, M. W., Andrew, R. M., Hauck, J., Olsen, A., et al. (2020). Global carbon budget 2020. *Earth System Science Data*, *12*(4), 3269–3340. https://doi.org/10.5194/essd-12-3269-2020

Friis, K., Körtzinger, A., Pätsch, J., & Wallace, D. W. R. (2005). On the temporal increase of anthropogenic CO_2 in the subpolar North Atlantic. *Deep Sea Research Part I: Oceanographic Research Papers*, *52*(5), 681–698. https://doi.org/10.1016/j.dsr.2004.11.017

Gao, H., Cai, W.-J., Jin, M., Dong, C., & Timmerman, A. H. V. (2022). Ocean ventilation Controls the contrasting anthropogenic CO_2 uptake rates between the western and eastern South Atlantic Ocean basins. *Global Biogeochemical Cycles*, *36*(6), e2021GB007265. https://doi.org/10.1029/2021GB007265

Gattuso, J.-P., Epitalon, J.-M., Lavinge, H., & Orr, J. C. (2020). Seacarb: Seawater carbonate chemistry. (Version R package version 3.2.13.). Retrieved from http://CRAN.R-project.org/package=seacarb

Goodkin, N. F., Levine, N. M., Doney, S. C., & Wanninkhof, R. (2011). Impacts of temporal CO_2 and climate trends on the detection of ocean anthropogenic CO_2 accumulation. *Global Biogeochemical Cycles*, *25*(3). https://doi.org/10.1029/2010GB004009

Gordon, A. L. (1981). South Atlantic thermocline ventilation. *Deep-Sea Research, Part A: Oceanographic Research Papers*, *28*(11), 1239–1264. https://doi.org/10.1016/0198-0149(81)90033-9

Gruber, N., Clement, D., Carter, B. R., Feely, R. A., van Heuven, S., Hoppema, M., et al. (2019). The oceanic sink for anthropogenic CO_2 from 1994 to 2007. *Science*, *363*(6432), 1193–1199. https://doi.org/10.1126/science.aau5153

Gruber, N., Landschützer, P., & Lovenduski, N. S. (2019). The variable southern ocean carbon sink. *Annual Review of Marine Science*, *11*(1), 159–186. https://doi.org/10.1146/annurev-marine-121916-063407

Gruber, N., Sarmiento, J. L., & Stocker, T. F. (1996). An improved method for detecting anthropogenic CO_2 in the oceans. *Global Biogeochemical Cycles*, *10*(4), 809–837. https://doi.org/10.1029/96GB01608

Hernández-Guerra, A., Talley, L. D., Pelegrí, J. L., Vélez-Belchí, P., Baringer, M. O., Macdonald, A. M., & McDonagh, E. L. (2019). The upper, deep, abyssal and overturning circulation in the Atlantic Ocean at 30°S in 2003 and 2011. *Progress in Oceanography*, *176*, 102136. https://doi.org/10.1016/j.pocean.2019.102136

Holte, J., Talley, L. D., Gilson, J., & Roemmich, D. (2017). An Argo mixed layer climatology and database. *Geophysical Research Letters*, *44*(11), 5618–5626. https://doi.org/10.1002/2017GL073426

Honisch, B., Ridgwell, A., Schmidt, D. N., Thomas, E., Gibbs, S. J., Sluijs, A., et al. (2012). The geological record of ocean acidification. *Science*, *335*(6072), 1058–1063. https://doi.org/10.1126/science.1208277

Ito, T., Follows, M. J., & Boyle, E. A. (2004). Is AOU a good measure of respiration in the oceans? *Geophysical Research Letters*, *31*(17). https://doi.org/10.1029/2004GL020900

Jackett, D. R., & McDougall, T. J. (1997). A neutral density variable for the World's oceans. *Journal of Physical Oceanography*, *27*(2), 237–263. https://doi.org/10.1175/1520-0485(1997)027<0237:ANDVFT>2.0.CO;2

Karstensen, J., Stramma, L., & Visbeck, M. (2008). Oxygen minimum zones in the eastern tropical Atlantic and Pacific oceans. *Progress in Oceanography*, *77*(4), 331–350. https://doi.org/10.1016/j.pocean.2007.05.009

Kelley, D., & Richards, C. (2022). oce: Analysis of oceanographic data. Retrieved from https://dankelley.github.io/oce/

Kitidis, V., Brown, I., Hardman-Mountford, N., & Lefèvre, N. (2017). Surface ocean carbon dioxide during the Atlantic Meridional Transect (1995–2013); evidence of ocean acidification. *Progress in Oceanography*, *158*, 65–75. https://doi.org/10.1016/j.pocean.2016.08.005

Koch, S. E., des Jardins, M., & Kocin, P. J. (1983). An interactive Barnes objective map analysis scheme for use with satellite and conventional data. *Journal of Applied Meteorology and Climatology*, *22*(9), 1487–1503. https://doi.org/10.1175/1520-0450(1983)022<1487:AIBOMA>2.0.CO;2

Koszalka, I. M., & Stramma, L. (2019). Current systems in the Atlantic Ocean. In J. K. Cochran, H. J. Bokuniewicz, & P. L. Yager (Eds.), *Encyclopedia of ocean sciences* (3rd edn, pp. 204–211). Academic Press. https://doi.org/10.1016/B978-0-12-409548-9.11291-6

Kulk, G., Platt, T., Dingle, J., Jackson, T., Jönsson, B. F., Bouman, H. A., et al. (2020). Primary production, an index of climate change in the ocean: Satellite-based estimates over two decades. *Remote Sensing*, *12*(5), 826. https://doi.org/10.3390/rs12050826

Lachkar, Z. (2014). Effects of upwelling increase on ocean acidification in the California and Canary Current systems. *Geophysical Research Letters*, *41*(1), 90–95. https://doi.org/10.1002/2013GL058726

Lamont, T., García-Reyes, M., Bograd, S. J., van der Lingen, C. D., & Sydeman, W. J. (2018). Upwelling indices for comparative ecosystem studies: Variability in the Benguela upwelling system. *Journal of Marine Systems*, *188*, 3–16. https://doi.org/10.1016/j.jmarsys.2017.05.007

Lauvset, S. K., Carter, B. R., Perez, F. F., Jiang, L.-Q., Feely, R. A., Velo, A., & Olsen, A. (2020). Processes driving global Interior Ocean pH distribution. *Global Biogeochemical Cycles*, *34*(1). https://doi.org/10.1029/2019GB006229

Lauvset, S. K., Lange, N., Tanhua, T., Bittig, H. C., Olsen, A., Kozyr, A., et al. (2021). An updated version of the global interior ocean biogeochemical data product, GLODAPv2.2021. *Earth System Science Data*, *13*(12), 5565–5589. https://doi.org/10.5194/essd-13-5565-2021

Lee, K., Choi, S.-D., Park, G.-H., Wanninkhof, R., Peng, T.-H., Key, R. M., et al. (2003). An updated anthropogenic CO_2 inventory in the Atlantic Ocean. *Global Biogeochemical Cycles*, *17*(4). https://doi.org/10.1029/2003GB002067

Lee, K., Kim, T.-W., Byrne, R. H., Millero, F. J., Feely, R. A., & Liu, Y.-M. (2010). The universal ratio of boron to chlorinity for the North Pacific and North Atlantic oceans. *Geochimica et Cosmochimica Acta*, *74*(6), 1801–1811. https://doi.org/10.1016/j.gca.2009.12.027

Levine, N. M., Doney, S. C., Wanninkhof, R., Lindsay, K., & Fung, I. Y. (2008). Impact of ocean carbon system variability on the detection of temporal increases in anthropogenic CO_2. *Journal of Geophysical Research*, *113*(C3), C03019. https://doi.org/10.1029/2007JC004153

Lueker, T. J., Dickson, A. G., & Keeling, C. D. (2000). Ocean pCO_2 calculated from dissolved inorganic carbon, alkalinity, and equations for K1 and K2: Validation based on laboratory measurements of CO_2 in gas and seawater at equilibrium. *Marine Chemistry*, *70*(1), 105–119. https://doi.org/10.1016/S0304-4203(00)00022-0

Manta, G., Speich, S., Karstensen, J., Hummels, R., Kersalé, M., Laxenaire, R., et al. (2021). The South Atlantic meridional overturning circulation and mesoscale Eddies in the first GO-SHIP section at 34.5°S. *Journal of Geophysical Research: Oceans*, *126*(2). https://doi.org/10.1029/2020JC016962

Meinshausen, M., Nicholls, Z. R. J., Lewis, J., Gidden, M. J., Vogel, E., Freund, M., et al. (2020). The shared socio-economic pathway (SSP) greenhouse gas concentrations and their extensions to 2500. *Geoscientific Model Development*, *13*(8), 3571–3605. https://doi.org/10.5194/gmd-13-3571-2020

Mémery, L., Arhan, M., Alvarez-Salgado, X. A., Messias, M.-J., Mercier, H., Castro, C. G., & Rios, A. F. (2000). The water masses along the Western boundary of the south and equatorial Atlantic. *Progress in Oceanography*, *47*(1), 69–98. https://doi.org/10.1016/S0079-6611(00)00032-X

Millero, F. J. (2007). The marine inorganic carbon cycle. *Chemical Reviews*, *107*(2), 308–341. https://doi.org/10.1021/cr0503557

Murata, A., Kumamoto, Y., Sasaki, K., Watanabe, S., & Fukasawa, M. (2008). Decadal increases of anthropogenic CO_2 in the subtropical South Atlantic ocean along 30°S. *Journal of Geophysical Research*, *113*(C6), C06007. https://doi.org/10.1029/2007JC004424

Orr, J. C., Epitalon, J.-M., Dickson, A. G., & Gattuso, J.-P. (2018). Routine uncertainty propagation for the marine carbon dioxide system. *Marine Chemistry*, *207*, 84–107. https://doi.org/10.1016/j.marchem.2018.10.006

Orr, J. C., Fabry, V. J., Aumont, O., Bopp, L., Doney, S. C., Feely, R. A., et al. (2005). Anthropogenic ocean acidification over the twenty-first century and its impact on calcifying organisms. *Nature*, *437*(7059), 681–686. https://doi.org/10.1038/nature04095

Orselli, I. B. M., Kerr, R., Ito, R. G., Tavano, V. M., Mendes, C. R. B., & Garcia, C. A. E. (2018). How fast is the Patagonian shelf-break acidifying? *Journal of Marine Systems*, *178*, 1–14. https://doi.org/10.1016/j.jmarsys.2017.10.007

Perez, F. F., & Fraga, F. (1987). Association constant of fluoride and hydrogen ions in seawater. *Marine Chemistry*, *21*(2), 161–168. https://doi.org/10.1016/0304-4203(87)90036-3

Poole, R., & Tomczak, M. (1999). Optimum multiparameter analysis of the water mass structure in the Atlantic Ocean thermocline. *Deep Sea Research Part I: Oceanographic Research Papers*, *46*(11), 1895–1921. https://doi.org/10.1016/S0967-0637(99)00025-4

Provost, C., Escoffier, C., Maamaatuaiahutapu, K., Kartavtseff, A., & Garçon, V. (1999). Subtropical mode waters in the South Atlantic Ocean. *Journal of Geophysical Research*, *104*(C9), 21033–21049. https://doi.org/10.1029/1999JC900049

Ríos, A. F., Resplandy, L., García-Ibáñez, M. I., Fajar, N. M., Velo, A., Padin, X. A., et al. (2015). Decadal acidification in the water masses of the Atlantic Ocean. *Proceedings of the National Academy of Sciences of the United States of America*, *112*(32), 9950–9955. https://doi.org/10.1073/pnas.1504613112

Ríos, A. F., Velo, A., Pardo, P. C., Hoppema, M., & Pérez, F. F. (2012). An update of anthropogenic CO2 storage rates in the western South Atlantic basin and the role of Antarctic bottom water. *Journal of Marine Systems*, *94*, 197–203. https://doi.org/10.1016/j.jmarsys.2011.11.023

Russell, J. L., & Dickson, A. G. (2003). Variability in oxygen and nutrients in South Pacific Antarctic intermediate water. *Global Biogeochemical Cycles*, *17*(2). https://doi.org/10.1029/2000GB001317

Sabine, C. L., Feely, R. A., Gruber, N., Key, R. M., Lee, K., Bullister, J. L., et al. (2004). The oceanic sink for anthropogenic CO_2. *Science*, *305*(5682), 367–371. https://doi.org/10.1126/science.1097403

Sabine, C. L., & Tanhua, T. (2010). Estimation of anthropogenic CO_2 inventories in the ocean. *Annual Review of Marine Science*, *2*(1), 175–198. https://doi.org/10.1146/annurev-marine-120308-080947

Salt, L. A., van Heuven, S. M. A. C., Claus, M. E., Jones, E. M., & de Baar, H. J. W. (2015). Rapid acidification of mode and intermediate waters in the southwestern Atlantic Ocean. *Biogeosciences*, *12*(5), 1387–1401. https://doi.org/10.5194/bg-12-1387-2015

Santos, G. C., Kerr, R., Azevedo, J. L. L., Mendes, C. R. B., & da Cunha, L. C. (2016). Influence of Antarctic intermediate water on the deoxygenation of the Atlantic Ocean. *Dynamics of Atmospheres and Oceans*, *76*, 72–82. https://doi.org/10.1016/j.dynatmoce.2016.09.002

Sarmiento, J. L., & Gruber, N. (2006). *Ocean biogeochemical dynamics*. Princeton University Press.

Sato, O. T., & Polito, P. S. (2014). Observation of South Atlantic subtropical mode waters with Argo profiling float data. *Journal of Geophysical Research: Oceans*, *119*(5), 2860–2881. https://doi.org/10.1002/2013JC009438

Schmidt, M., & Eggert, A. (2016). Oxygen cycling in the northern Benguela Upwelling System: Modelling oxygen sources and sinks. *Progress in Oceanography*, *149*, 145–173. https://doi.org/10.1016/j.pocean.2016.09.004

Schmidtko, S., Stramma, L., & Visbeck, M. (2017). Decline in global oceanic oxygen content during the past five decades. *Nature*, *542*(7641), 335–339. https://doi.org/10.1038/nature21399

Stramma, L., & England, M. (1999). On the water masses and mean circulation of the South Atlantic Ocean. *Journal of Geophysical Research*, *104*(C9), 20863–20883. https://doi.org/10.1029/1999JC900139

Takahashi, T., Sutherland, S. C., Chipman, D. W., Goddard, J. G., Ho, C., Newberger, T., et al. (2014). Climatological distributions of pH, pCO_2, total CO_2, alkalinity, and CaCO3 saturation in the global surface ocean, and temporal changes at selected locations. *Marine Chemistry*, *164*, 95–125. https://doi.org/10.1016/j.marchem.2014.06.004

Talley, L. D., Feely, R. A., Sloyan, B. M., Wanninkhof, R., Baringer, M. o., Bullister, J. L., et al. (2016). Changes in Ocean heat, carbon content, and ventilation: A review of the first decade of GO-SHIP global repeat hydrography. *Annual Review of Marine Science*, *8*(1), 185–215. https://doi.org/10.1146/annurev-marine-052915-100829

Tanhua, T., Hoppema, M., Jones, E. M., Stöven, T., Hauck, J., Dávila, M. G., et al. (2017). Temporal changes in ventilation and the carbonate system in the Atlantic sector of the southern ocean. *Deep Sea Research Part II: Topical Studies in Oceanography*, *138*, 26–38. https://doi.org/10.1016/j.dsr2.2016.10.004

Tanhua, T., & Keeling, R. F. (2012). Changes in column inventories of carbon and oxygen in the Atlantic Ocean. *Biogeosciences*, *9*(11), 4819–4833. https://doi.org/10.5194/bg-9-4819-2012

Touratier, F., & Goyet, C. (2004). Applying the new TrOCA approach to assess the distribution of anthropogenic CO_2 in the Atlantic Ocean. *Journal of Marine Systems*, *46*(1–4), 181–197. https://doi.org/10.1016/j.jmarsys.2003.11.020

Vázquez-Rodríguez, M., Pérez, F. F., Velo, A., Ríos, A. F., & Mercier, H. (2012). Observed acidification trends in North Atlantic water masses. *Biogeosciences*, *9*(12), 5217–5230. https://doi.org/10.5194/bg-9-5217-2012

Wallace, D. W. R. (1995). *Monitoring global ocean carbon inventories*. Ocean Observing System Development Panel.

Wallace, D. W. R. (2001). Chapter 6.3 Storage and transport of excess CO2 in the oceans: The JGOFS/WOCE global CO_2 survey. In *International Geophysics*, G. Siedler, J. Church, & J. Gould (Eds.) (Vol. 77). Academic Press. https://doi.org/10.1016/S0074-6142(01)80136-4

Wanninkhof, R., Doney, S. C., Bullister, J. L., Levine, N. M., Warner, M., & Gruber, N. (2010). Detecting anthropogenic CO_2 changes in the interior Atlantic Ocean between 1989 and 2005. *Journal of Geophysical Research*, *115*(C11), C11028. https://doi.org/10.1029/2010JC006251

Waters, J. F., Millero, F. J., & Sabine, C. L. (2011). Changes in South Pacific anthropogenic carbon. *Global Biogeochemical Cycles*, *25*(4). https://doi.org/10.1029/2010GB003988

Waugh, D. W., Primeau, F., De Vries, T., & Holzer, M. (2013). Recent changes in the ventilation of the southern oceans. *Science*, *339*(6119), 568–570. https://doi.org/10.1126/science.1225411

Williams, N. L., Feely, R. A., Sabine, C. L., Dickson, A. G., Swift, J. H., Talley, L. D., & Russell, J. L. (2015). Quantifying anthropogenic carbon inventory changes in the Pacific sector of the Southern Ocean. *Marine Chemistry*, *174*, 147–160. https://doi.org/10.1016/j.marchem.2015.06.015

Wolf-Gladrow, D. A., Zeebe, R. E., Klaas, C., Körtzinger, A., & Dickson, A. G. (2007). Total alkalinity: The explicit conservative expression and its application to biogeochemical processes. *Marine Chemistry*, *106*(1), 287–300. https://doi.org/10.1016/j.marchem.2007.01.006

Woosley, R. J. (2021). Evaluation of the temperature dependence of dissociation constants for the marine carbon system using pH and certified reference materials. *Marine Chemistry*, *229*, 103914. https://doi.org/10.1016/j.marchem.2020.103914

Woosley, R. J., Millero, F. J., & Wanninkhof, R. (2016). Rapid anthropogenic changes in CO_2 and pH in the Atlantic Ocean: 2003–2014. *Global Biogeochemical Cycles*, *21*(1), 70–90. https://doi.org/10.1002/2015gb005248

Xue, L., Yu, W., Wang, H., Jiang, L.-Q., Feng, L., Gao, L., et al. (2014). Temporal changes in surface partial pressure of carbon dioxide and carbonate saturation state in the eastern equatorial Indian Ocean during the 1962–2012 period. *Biogeosciences*, *11*(22), 6293–6305. https://doi.org/10.5194/bg-11-6293-2014

Zeebe, R. E., & Wolf-Gladrow, D. (Eds.) (2001). *Chapter 1 equilibrium*, (Vol. 65, pp. 1–84). Elsevier Oceanography Series. https://doi.org/10.1016/S0422-9894(01)80002-7

References From the Supporting Information

Bittig, H. C., Steinhoff, T., Claustre, H., Fiedler, B., Williams, N. L., Sauzède, R., et al. (2018). An alternative to static climatologies: Robust estimation of open ocean CO_2 variables and nutrient concentrations from T, S, and O_2 data using bayesian neural networks. *Frontiers in Marine Science*, *5*, 328. https://doi.org/10.3389/fmars.2018.00328

Friis, K., Körtzinger, A., & Wallace, D. W. R. (2003). The salinity normalization of marine inorganic carbon chemistry data. *Geophysical Research Letters*, *30*(2). https://doi.org/10.1029/2002GL015898

Orselli, I. B. M., Goyet, C., Kerr, R., de Azevedo, J. L., Araujo, M., Galdino, F., et al. (2019). The effect of Agulhas Eddies on absorption and transport of anthropogenic carbon in the south Atlantic Ocean. *Climate*, *7*(6), 84. https://doi.org/10.3390/cli7060084

Venables, W. N., & Ripley, B. D. (2002). *Modern applied statistics with S (fourth)*. Springer. Retrieved from http://www.stats.ox.ac.uk/pub/MASS4/